Integrated Type and Approximate Dimensional Synthesis of Four-Bar Planar Mechanisms for Rigid Body Guidance

by

Timothy J. Luu, B.A.Sc.

Carleton University

A thesis submitted to

the Faculty of Graduate Studies and Research

in partial fulfillment of

the requirements for the degree of

Master of Applied Science

Ottawa-Carleton Institute for

Mechanical and Aerospace Engineering

Department of

Mechanical and Aerospace Engineering

Carleton University

Ottawa, Ontario

June 16, 2005

The undersigned recommend to

the Faculty of Graduate Studies and Research

acceptance of the thesis

Integrated Type and Approximate Dimensional Synthesis of Four-Bar Planar Mechanisms for Rigid Body Guidance

submitted by **Timothy J. Luu, B.A.Sc.**

in partial fulfillment of the requirements for

the degree of Master of Applied Science

Dr. M. J. D. Hayes
Thesis Supervisor

Dr. J. C. Beddoes
Chair, Department of
Mechanical and Aerospace Engineering

Carleton University

June 16, 2005

Abstract

A method is presented that integrates type and approximate dimensional synthesis of planar four-bar mechanisms for rigid-body guidance. In this work, the term *four-bar mechanism* denotes a linkage comprised of any two of RR, PR, RP, and PP dyads. As a precursor, attempts are made to linearize this particular synthesis problem such that linear algebra techniques may be applied to obtain a solution. This method uses kinematic mapping to map planar displacements to three dimensional coordinates in a projective image space. Limited success is achieved in this regard. An improved novel approach is then developed by correlating the positions of key points of the mechanism in two different coordinate frames. By doing so, the number of independent variables defining a suitable dyad for the desired rigid-body guidance is reduced from five to two. After applying these geometric constraints, numerical methods are used to size link lengths, locate joint axes, and decide between RR, PR, RP and PP dyads that, when combined, guide a rigid body through the best approximation, in a least squares sense, of n specified positions and orientations, where $n \geq 5$. No initial guesses of type or dimension are required. Several examples are presented illustrating the effectiveness and robustness of this new approach.

Acknowledgements

I would like to thank Dr. John Hayes for his dedicated supervision of this work. In my perspective, he has made theoretical kinematics not only understandable, but also enjoyable.

I would also like to thank the unwavering support of my wife, Rachel. I can only hope to support your research as much as you have supported mine.

to Rachel,

who keeps me sane and loved.

Contents

List of Figures

List of Tables

Claim of Originality

Certain aspects of the procedure for integrated type and approximate dimensional synthesis of planar four-bar mechanisms for rigid-body guidance are presented herein for the first time. The following contributions are of particular interest:

1. The linearization of the synthesis matrix to facilitate the application of singular value decomposition for the search of approximate solutions.

2. The method of correlating points on the fixed coordinate frame Σ with the moving coordinate frame E as a means to reduce the number of unknown parameters in the synthesis matrix from five to two.

3. The application of Nelder-Mead minimization and singular value decomposition to solve for the remaining three unkown parameters, once the two parameters are found.

4. The study of accuracy and robustness of the aforementioned algorithm for the approximate synthesis of planar four-bar mechanisms of varying types.

Some of these results have appeared in two refereed publications: [1, 2].

Chapter 1

Introduction

1.1 Background

The planar four-bar mechanism is arguably the simplest closed-loop kinematic chain, and has a wide variety of applications such as windshield wipers, fan oscillators, landing gears, steering linkages, suspension linkages, vice grips, etc. In this thesis, the term *four-bar mechanism* means a linkage comprised of any two of RR, PR, RP, and PP dyads. The kinematic synthesis of planar four-bar mechanisms for rigid body guidance was proposed by Burmester [3]. The theory presented by Burmester stated that five finitely separated poses (positions and orientations) of a rigid body define a planar four-bar mechanism that can guide a rigid body exactly through those five poses. Burmester showed that the problem leads to at most four dyads that, when paired, determine at most six different four-bar mechanisms that can guide the rigid body exactly through the poses.

A dyad is a pairing of two joints. For planar mechanisms, the types of joints are limited to two: revolute (R) and prismatic (P). The pairing of the two types then leads to four possible dyads: revolute-revolute (RR), prismatic-revolute (PR), revolute-prismatic (RP), and prismatic-prismatic (PP). Figure 1.1 illustrates the four dyads.

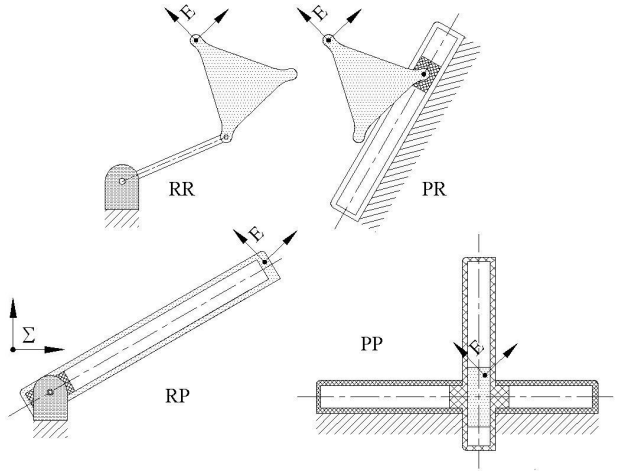

Figure 1.1: The four planar dyads.

Although the solution to the Burmester problem yields mechanisms that have no deviation from the prescribed poses, a major disadvantage is that only five positions and associated orientations may be prescribed. The designer has no control over how the mechanism behaves for any intermediate poses. For motion generation with relatively long travel, it would be advantageous to have a means by which a mechanism can be synthesized that guides a rigid body through n prescribed poses, with $n > 5$. In general, an exact solution does not exist to this problem. The problem then becomes that of approximate synthesis, where the mechanism determined to be the solution will guide a rigid-body through the prescribed poses with the smallest error, typically in a least squares sense. The approximate solution will be unique up to the error minimization criteria.

Kinematic synthesis involves three aspects: number synthesis; type synthesis; and dimensional synthesis. Number synthesis determines the number of joints connecting the links in the mechanism, or the number of links. Type synthesis involves choosing the type of dyads used in the mechanism, whether they be RR, PR, RP, or PP. Dimensional synthesis involves sizing the dimensions of each link in the mechanism. In general, studies on approximate kinematic synthesis only consider dimensional synthesis, while assuming a particular type.

Until now, there has been no successful and robust method to integrate both type and approximate dimensional synthesis of planar four-bar mechanisms for rigid body guidance, without apriori knowledge or initial guesses. This thesis presents a method for doing so for planar four-bar mechanisms. This will allow mechanism designers to stop designing mechanisms iteratively, by trial and error, but rather directly design the optimal mechanism from a least-squares standpoint. First, a literature review is presented of the previous methods developed for approximate synthesis.

1.2 Literature Review

The following is a literature review of the methods proposed for approximate kinematic synthesis of planar four-bar mechanisms for rigid-body guidance.

Several methods focus on linkage optimization, which requires an initial linkage that approximates the desired motion. The linkage is then optimized using this method to become a better approximation of the desired motion. Methods developed for this purpose include nonlinear optimization, which starts out with an initial guess mechanism that can be deformed [4, 5, 6]. The error function is then formulated to be based on the amount that the mechanism needs to be deformed to exactly generate the prescribed poses. The mechanism that least needs to be deformed will be the optimum mechanism according to this criterion.

Another method involves unconstrained nonlinear least-square optimization, which uses separation of variables to decouple the configuration variables from the linkage parameters [7]. The problem is then formulated as an unconstrained overdetermined system of nonlinear algebraic equations whose least-square approximation is computed by the Newton-Gauss method.

Another method combines differential evolution, an evolutionary optimization scheme

that can search outside the initial defined bounds for the design variables, and the method of geometric centroid of precision positions [8]. The combination of these two methods leads to two penalty functions being used, one for constraint violation and one for relative accuracy, which, when combined, improves the desired accuracy level.

The method of non-linear goal programming applies multiple objective optimization techniques to perform optimal synthesis [9]. In this method, the objectives of the mechanism are first identified and prioritized according to their relative importance. The design variables are then identified and their relationships to the dependent variables are established. Non-linear goal programming is then employed to determine the optimal values for the design variables that best satisfy the desired objectives of the problem. This enables the ability to include all the objectives directly in the optimization process.

A method using an approximate bi-invariant metric introduces an approximating sphere to measure the errors of position and orientation of a guided rigid body, rather than planar error measurements [10, 11]. The errors are then measured using a bi-invariant metric in the image space of spherical displacements, and are minimized for each of the prescribed poses.

Two methods employ the use of exact-gradients to optimize planar mechanisms [12, 13]. This removes the difficulties in calculating the partial derivatives necessary for optimization, while still using Cartesian coordinates. The optimization is then formulated using algebraic constraint equations, allowing the use of a large number of prescribed poses.

A method using interior-points provides an alternative to formulating problems with linear constraints and an objective function formed as a sum of squared quantities [14]. Computational results have demonstrated that the algorithm is able to find an approximate optimal solution in fewer iterations and function evaluations compared to its conventional counterpart.

A method using parametric constraints uses a parametrization of the mechanisms syn-

thesis variables [15]. Using this technique, non-linear minimization can then be used to optimize a wide variety of mechanisms including planar, spherical, and spatial.

Finally, a method using kinematic constraints uses prescribed position, velocity, acceleration, or jerk [16]. The optimization method then minimizes a sequence of quadratic equations.

Other methods do not rely on initial guesses. Wang, Yu, Tang, and Li have developed a guidance-line rotation method of synthesizing mechanisms for rigid-body guidance [17]. Yao and Angeles have employed the contour method in an attempt to find all dyads corresponding to minima of the objective function for approximate synthesis [18]. In this method, the underlying normal equations of the optimization problem are obtained and then reduced to a set of two bivariate polynomial equations. These two equations are then plotted as two contours, whose intersections represent all the minima of the objective function of the synthesis problem. Lui and Yang use the continuation method to find all solutions corresponding to minima of the objeective function for approximate synthesis [19]. In this method, the approximate synthesis problem is reduced to a set of polynomial equations. Polynomial continuation is used to find all the minima. Kong uses a similar approach, but using generalized inverse matrices to obtain the polynomial equations [20]. Modak proposed a method for kinematic synthesis given six poses using a moving Burmester point [21]. Kramer developed the selective precision synthesis technique for planar four-bar rigid body guidance [22]. This technique allows the designer to choose the precision of each pose, making poses more or less constrained as desired. The techique was modified by Kim to use displacement matrices. This allowed the application of the technique to slider-crank mechanisms [23].

The field of artificial intelligence has also been applied to solve the problem of approximate synthesis. Vasiliu and Yannou have developed a method using neural networks to synthesize planar mechanisms [24], as have Hoskins and Kramer [25]. Roston and Sturges

have developed a method using genetic algorithms to search for four-bar mechanisms [26], as have Cabrera, Simon, and Prado [27]. Ekart and Markus combined genetic algorithms and decision tree learning methods to create a learning engine that, after sufficient linkage data is inputted, finds desired linkages by constructive induction. Bose, Gini, and Riley have developed a similar method using a case-based approach to store and retrieve design cases of four-bar linkages [28]. Adaptation methods are then used on the stored data to find linkages that fit new design criteria. Wu has developed a method for designing four bar linkages for rigid-body guidance with prescribed timing by using harmonic characteristic parameters of the coupler's rotation-angle function [29, 30]. This method tries to establish a relationship between rigid-body guidance with prescribed timing and the coupler's harmonic rotation. This method relies on a database of coupler harmonic rotations to establish this relationship.

Finally, kinematic mapping has been applied to approximate kinematic synthesis. Kinematic mapping, introduced by Blaschke and Grunwald [31, 32], maps planar displacements (translation and rotation) to points in a three dimensional image space. Ravani was the first to propose kinematic mapping for the application of approximate kinematic synthesis [33, 34]. Although this method does well in solving the five position Burmester problem [35, 36], limited success has been found in its application to approximate synthesis [1]. However, inspiration has been found through this technique that has led to a successful method for integrated type and appoximate dimensional synthesis, and is presented in Chapter 4.

The next chapter further investigates the application of kinematic mapping to approximate synthesis, and proposes a method to linearize the problem.

Chapter 2

Kinematics of Planar Four-Bar Mechanisms

This chapter details the relevant theory regarding kinematics of planar four-bar mechanisms. Discussions on homoegeneous coordinates and imaginary circular points are presented. Then, the associated principles are applied to find the algebraic coupler curve equation of a general planar four-bar mechanism.

2.1 Homogeneous Coordinates

Homogeneous coordinates add a coordinate w to the conventional Cartesian coordinates: (x, y) for planar coordinates, and (x, y, z) for spatial coordinates. The planar coordinates then become $(\frac{x}{w}, \frac{y}{w})$, and the spatial coordinates are $(\frac{x}{w}, \frac{y}{w}, \frac{z}{w})$. In this way, w acts as a scaling factor.

The utility of homogeneous coordinates is illustrated by the following problem. A straight line in the plane intersects an n^{th} order algebraic curve in at most n points [37]. These intersections include:

- touching the curve, which is equivalent to intersecting the curve twice or more,
- intersections at imaginary points,
- intersections at infinity.

Exceptions arise when $n = 1$ and the line and curve are coincident, and when the curve is degenerate.

By extension, two coplanar algebraic curves of orders n_a and n_b in general intersect in at most $n_a n_b$ points. Exceptions arise when the two curves are completely coincident, or when they share common portions. A problem arises for two distinct circles (two curves of order two), as they intersect in at most two real points. The following section identifies the missing two imaginary points using homogenous coordinates.

2.2 The Imaginary Circular Points

The general equation of a circle in Cartesian coordinates with centre (a, b) and radius r is

$$(x - a)^2 + (y - b)^2 - r^2 = 0. \tag{2.1}$$

Using homogenous coordinates, Equation (2.1) becomes

$$\left(\frac{x}{w} - a\right)^2 + \left(\frac{y}{w} - b\right)^2 - r^2 = 0. \tag{2.2}$$

Multiplying both sides by w^2 gives

$$(x - aw)^2 + (y - bw)^2 - r^2 w^2 = 0. \tag{2.3}$$

When $w = 1$, Equations (2.1) and (2.2) are equivalent. When $w = 0$, the circle is infinitely enlarged. In this case, the linear equation $w = 0$ represents the line at infinity in the projective plane, analogous to the lines $x = 0$ and $y = 0$ in the Euclidean plane. With $w = 0$, Equation (2.3) yields

$$x^2 + y^2 = 0, \tag{2.4}$$

which can be factored into

$$(x + iy)(x - iy) = 0. \tag{2.5}$$

Therefore, the line at infinity meets the circle on the two points

$$\begin{aligned} x &= iy \\ x &= -iy, \end{aligned} \tag{2.6}$$

with $w = 0$ in both cases.

These complex conjugate points are called the imaginary circular points in the plane, and are denoted I and J. Since Equations (2.5) and (2.6) do not contain a, b, or r, all circles contain I and J. These two imaginary circular points complete the four possible points of intersection between two circles.

Because a circle contains I and J once, a circle is said to have a circularity of one. In the following section, it will be shown that the coupler curve of a four-bar linkage in its most general form has a circularity of at most three [37].

2.3 The Coupler Curves of Planar Four-Bar Linkages

In this section, the algebraic formulation for the coupler curve of planar four-bar mechanisms is presented, as taken from [37]. For a full derivation, see [37, 38, 39, 40]. Consider

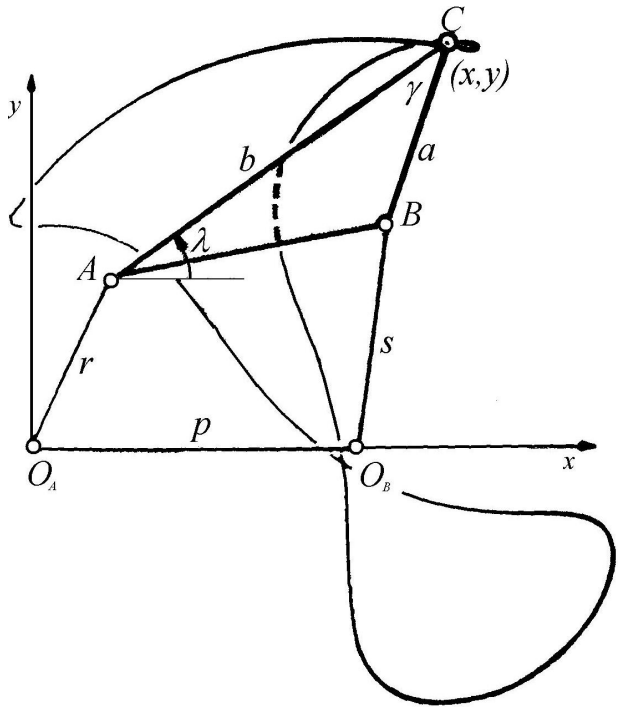

Figure 2.1: A general planar four-bar mechanism [37].

the planar four-bar linkage shown in Figure 2.1. The equation for its coupler curve is:

$$U^2 + V^2 = W^2, \tag{2.7}$$

where

$$\begin{aligned} U &= bx\Big(s^2 - \big((x-p)^2 + y^2 + a^2\big)\Big) - a\Big(y\sin\gamma + (x-p)\cos\gamma\Big)\Big(r^2 - (x^2+y^2+b^2)\Big), \\ V &= a\Big(y\cos\gamma - (x-p)\sin\gamma\Big)\Big(r^2 - (x^2+y^2+b^2)\Big) - by\Big(s^2 - \Big((x-p)^2 + y^2 + a^2\Big)\Big), \\ W &= 2ab\Big((x\,(x-p) + y^2)\sin\gamma - py\cos\gamma\Big). \end{aligned} \tag{2.8}$$

By expressing Equation (2.8) in homogeneous coordinates, the intersection of the coupler curve with the line at infinity can be found. Substituting $\frac{x}{w}$ and $\frac{y}{w}$ for x and y

respectively and setting $w = 0$ yields

$$\begin{aligned} U &= (x^2 + y^2)\left(a\left(y\sin\gamma + x\cos\gamma\right) - bx\right), \\ V &= (x^2 + y^2)\left(by - a\left(y\cos\gamma - x\sin\gamma\right)\right), \\ W &= 0. \end{aligned} \tag{2.9}$$

The intersections with the line at infinity are given by the constraints

$$\begin{aligned} w = 0, \\ U^2 + V^2 = 0, \end{aligned} \tag{2.10}$$

which, when applied to Equation (2.9), yields

$$\left(x^2 + y^2\right)^3 \left(a^2 + b^2 - 2ab\cos\gamma\right) = 0. \tag{2.11}$$

The second factor in Equation (2.11) is the Cosine Rule, which, in this case is

$$\left(a^2 + b^2 - 2ab\cos\gamma\right) = (AB)^2. \tag{2.12}$$

Equation (2.12) can only be zero when the points A and B in Figure 2.1 are coincident. This leads to the trivial case where the path of C becomes a circle about the points A and B, as they are coincident. Therefore, the intersections of the line at infinity with a non-degenerate coupler curve are given by:

$$\left(x^2 + y^2\right)^3 = 0. \tag{2.13}$$

The coupler curve intersects the line at infinity at the imaginary circular points I and J as found in Equation (2.6). Because Equation (2.13) is cubed, the points of intersection are triple points. Furthermore, as discussed in Section 2.2, all circles in the plane also

Mechanism	Coupler Curve Order	Circularity
General Four-Bar ($RRRR$)	6	3
Slider-Crank ($PRRR$)	4	1
Elliptic Trammel ($PRRP$)	2	0

Table 2.1: Coupler curves of different mechanism types [41].

contain the points I and J. Therefore, the coupler curve intersects all circles triply at the points I and J. The coupler curve is thus said to have a circularity of three, and in the most general case is said to be a tricircular sextic. Finally, since according to Equation (2.13), no sextic coupler curve can have a circularity higher than three, full circularity is three.

Full circularity can only occur in $RRRR$ type mechanisms. In this sense $RRRR$ types are the most general planar four-bar mechanisms. For mechanisms having prismatic joints, circularity is decreased. As a result, the order of the coupler curve is also decreased. A summary of these results for the most common types of planar four-bar mechanisms is given in Table 2.1. A complete table for all types of planar four-bar mechanisms is found in [41].

Chapter 3

Kinematic Mapping

In this chapter, the theory of kinematic synthesis using kinematic mapping is presented. Once the theory of kinematic mapping is given, its application to kinematic synthesis is detailed. In particular, RR and PR dyads are related to their corresponding quadric constraint surfaces in the image space. A procedure is then presented for finding a solution that integrates type and dimension synthesis using image space geometry. Singular value decomposition theory is then also presented to aid in understanding the numerical implications of the synthesis problem. Finally, attempts are made in finding a solution using this method for RR and PR dyads.

3.1 Kinematic Mapping Theory

Kinematic mapping was introduced independently by Blaschke and Grunwald in 1911 [31, 32]. It is used to map planar displacements in the Euclidean plane to points in a three dimensional projective image space. All relative planar displacements of two rigid bodies can be considered as the relative displacement of two Cartesian reference coordinate frames, E and Σ, with E attached to one rigid body and Σ attached to the other. Without loss of generality, Σ may be considered fixed with E free to move.

Homogeneous coordinates of points in E are given by the ratios $(x : y : z)$. The same points in Σ are given by the ratios $(X : Y : Z)$. The relationship between the two reference frames is given by the homogeneous transformation

$$\begin{bmatrix} X \\ Y \\ Z \end{bmatrix} = \begin{bmatrix} \cos\theta & -\sin\theta & a \\ \sin\theta & \cos\theta & b \\ 0 & 0 & 1 \end{bmatrix} \begin{bmatrix} x \\ y \\ z \end{bmatrix}, \tag{3.1}$$

where (a, b) are the $(\frac{X}{Z}, \frac{Y}{Z})$ Cartesian coordinates of the origin of E with respect to Σ, and θ is the orientation of E relative to Σ. Any point $(x : y : z)$ in E can be mapped to $(X : Y : Z)$ in Σ using this transformation.

A planar displacement is defined as any combination of planar translations and rotations. All planar displacements can be represented by a single rotation through an angle about an axis normal to the plane of displacement. Even a pure translation may be considered as a rotation through an infinitesimal angle about the point at infinity in the direction normal to the translation [36]. The coordinates of the rotation axis are defined as the pole of the displacement.

The pole coordinates for a planar displacement are obtained from the eigenvector corresponding to the one real eigenvalue of the transformation matrix in Equation (3.1). Because the pole coordinates are derived from the eigenvector of the transformation in Equation (3.1), they are invariant under the transformation. The coordinates of the pole are then the same in both reference frames. It can be shown that the pole coordinates are

$$\begin{aligned} X_p = \quad x_p = \quad & a\sin\frac{\theta}{2} - b\cos\frac{\theta}{2}, \\ Y_p = \quad y_p = \quad & a\cos\frac{\theta}{2} + b\sin\frac{\theta}{2}, \\ Z_p = \quad z_p = \quad & 2\sin\frac{\theta}{2}. \end{aligned} \tag{3.2}$$

The value of the homogenizing coordinate is arbitrary, and, without loss in generality, may be set to $Z_p = z_p = 2\sin\frac{\theta}{2}$.

The intent of kinematic mapping is to map these homogeneous coordinates to points of a three dimensional projective image space, in terms of the parameters that characterize the displacement, (a, b, θ). The image space coordinates are defined to be

$$\begin{aligned} X_1 &= a\sin\frac{\theta}{2} - b\cos\frac{\theta}{2}, \\ X_2 &= a\cos\frac{\theta}{2} + b\sin\frac{\theta}{2}, \\ X_3 &= 2\sin\frac{\theta}{2}, \\ X_4 &= 2\cos\frac{\theta}{2}. \end{aligned} \tag{3.3}$$

Since each distinct displacement described by (a, b, θ) has a corresponding unique image point, the inverse mapping can be obtained. For a given point of the image space, the displacement parameters are

$$\begin{aligned} \tan\frac{\theta}{2} &= \frac{X_3}{X_4}, \\ a &= \frac{2(X_1X_3 + X_2X_4)}{X_3^2 + X_4^2}, \\ b &= \frac{2(X_2X_3 - X_1X_4)}{X_3^2 + X_4^2}. \end{aligned} \tag{3.4}$$

The mapping from the Euclidean plane to the image space is injective. This means that although all Euclidean displacements can be represented in the image space, not all image space points represent actual Cartesian displacements. One can deduce from Equation (3.4) that points in the image space such that $X_3^2 + X_4^2 = 0$ do not represent displacements in the Euclidean plane.

Equation (3.1) and Equation (3.3) may be combined to express a displacement of E

with respect to Σ as an image point [41], such that

$$\lambda \begin{bmatrix} X \\ Y \\ Z \end{bmatrix} = \begin{bmatrix} X_4^2 - X_3^2 & -2X_3X_4 & 2(X_1X_3 + X_2X_4) \\ 2X_3X_4 & X_4^2 - X_3^2 & 2(X_2X_3 - X_1X_4) \\ 0 & 0 & X_3^2 + X_4^2 \end{bmatrix} \begin{bmatrix} x \\ y \\ z \end{bmatrix}. \tag{3.5}$$

The inverse transformation can also be obtained by inverting the matrix in Equation (3.5)

$$\gamma \begin{bmatrix} x \\ y \\ z \end{bmatrix} = \begin{bmatrix} X_4^2 - X_3^2 & 2X_3X_4 & 2(X_1X_3 - X_2X_4) \\ -2X_3X_4 & X_4^2 - X_3^2 & 2(X_2X_3 + X_1X_4) \\ 0 & 0 & X_3^2 + X_4^2 \end{bmatrix} \begin{bmatrix} X \\ Y \\ Z \end{bmatrix}. \tag{3.6}$$

Note that λ and γ are arbitrary scaling factors arising from the use of homogeneous coordinates.

3.2 Kinematic Constraints in the Image Space

All constrained planar motions are a result of guidance from a pairing of specific types of planar dyads, a dyad being a linkage with one type of two possible joints on the proximal and distal ends. The two possibilities are revolute (R), which allows a rotational degree of freedom, and prismatic (P), which allows a translational degree of freedom. The four possibilities for dyads then become:

- RR: Forcing a point with fixed coordinates in E to move on a fixed circle in Σ.
- PR: Forcing a point with fixed coordinates in E to move on a fixed line in Σ.
- RP: Forcing a line with fixed coordinates in E to move on a fixed point in Σ.
- PP: Forcing a line with fixed coordinates in E to move in the direction of a fixed line in Σ.

The circular constraint of an RR dyad is considered the most general, as a line can be considered a special case of a circle, having an infinite radius centred at infinity. The linear constraints of PR and RP dyads are kinematic inversions of one another. A PR dyad becomes an RP dyad by considering Σ to be moving with respect to E, instead of vice versa. The PP dyad is a special case of the PR and RP dyads. Since no rotation in a PP dyad is possible, it becomes a degenerate case which makes its kinematics trivial.

A planar displacement in the Euclidean plane maps to a point in the image space. A motion is a continuous set of displacements. Therefore, a motion will map to a continuous set of points in the image space, defining a curve. As shown in [42], the constraints imposed by the four different dyad types are quadric surfaces with special properties in the image space.

Substituting a Euclidean displacement from Equation (3.5) into the general equation of a circle yields

$$K_0(X^2+Y^2)+2K_1XZ+2K_2YZ+K_3Z^2 = 0. \tag{3.7}$$

The K_i in Equation (3.7) define the constraint imposed by the dyad. This equation implies that the constraint surfaces corresponding to all four dyads can be represented by one equation [43]. This equation is obtained by expanding Equation (3.5) and substituting the results into Equation (3.7). Simplifications may be made by assuming:

1. It is not necessary to consider displacements at infinity. This assumption is reasonable since no practical mechanism can guide a rigid body to infinity. Therefore, since we do not have to consider the case of $z = 0$, we are able to set $z = 1$ without loss of generality, since z is an arbitrary homogenizing variable.

2. Rotations of $\theta = \pi$ radians are removed as a possibility. This assumption is necessary to normalize the homogenizing variable X_4, similar to the first assumption. Rotations

of π radians correspond to points in the image space in the plane $X_4 = 0$. In this special case, the image space coordinates are, using Equation (3.3),

$$\begin{aligned} X_1 &= a, \\ X_2 &= b, \\ X_3 &= 2, \\ X_4 &= 0. \end{aligned} \tag{3.8}$$

Removing this special case allows the image space coordinates to be normalized by setting $X_4 = 1$. This implies dividing the X_i by $X_4 = 2\cos\frac{\theta}{2}$, giving

$$\begin{aligned} X_1 &= \frac{1}{2}\left(a\tan\left(\theta/2\right) - b\right), \\ X_2 &= \frac{1}{2}\left(a + b\tan\left(\theta/2\right)\right), \\ X_3 &= \tan\left(\theta/2\right), \\ X_4 &= 1. \end{aligned} \tag{3.9}$$

Applying these assumptions to Equation (3.5) and (3.6) and substituting both into Equation (3.7) gives the general constraint surface equation [43]

$$\begin{aligned} &K_0(X_1^2 + X_2^2) + (-K_0x + K_1)X_1X_3 + (-K_0y + K_2)X_2X_3 \mp (K_0y + K_2)X_1 \\ &\pm(K_0x + K_1)X_2 \mp (K_1y - K_2x)X_3 + \tfrac{1}{4}[K_0(x^2 + y^2) - 2(K_1x + K_2y) \\ &+K_3]X_3^2 + \tfrac{1}{4}[K_0(x^2 + y^2) + 2(K_1x + K_2y) + K_3] = 0. \end{aligned} \tag{3.10}$$

For RR and PR dyads the X_i are the image space coordinates that represent the displacement of E relative to Σ, and x and y are the Cartesian coordinates of the coupler attachment point in E. In this case, the upper signs are used. This equation defines a

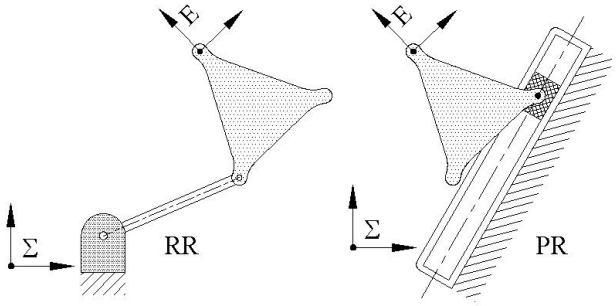

Figure 3.1: An RR and PR dyad.

quadric three dimensional surface. Depending on the dyad type, the surface will have distinct properties. For both the RR and PR dyads, the rigid body is joined to the dyad by a revolute joint, as shown in Figure 3.1. The x and y for each of these types of dyads is then the location of the revolute centre of the attachment joint. The constraint surfaces for these dyads require the upper signs in Equation (3.10). For RP dyads, the kinematic constraint is inverted, as shown in Figure 3.2. The rigid body is joined to the dyad by a prismatic joint, and the revolute joint is fixed in Σ. For this case, the x and y in Equation (3.10) are replaced with X and Y and the lower signs are used. For PP dyads as illustrated in Figure 3.3, the constraint surface equation is trivial. Since θ, the angle of E relative to Σ, is constant, so is X_3. In PP dyads a and b are unconstrained. This makes X_1 and X_2 unconstrained. The equation then is solely dependent on θ, making the constraint surface

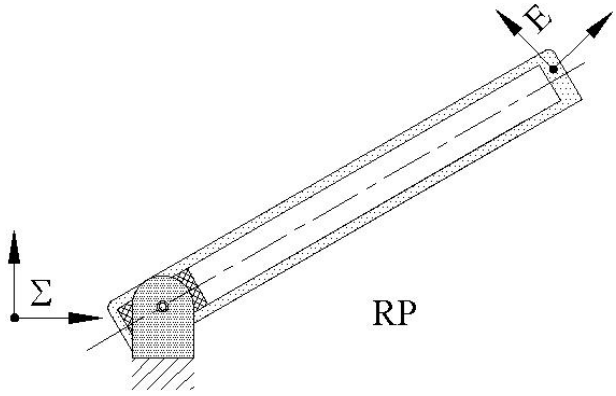

Figure 3.2: An RP dyad.

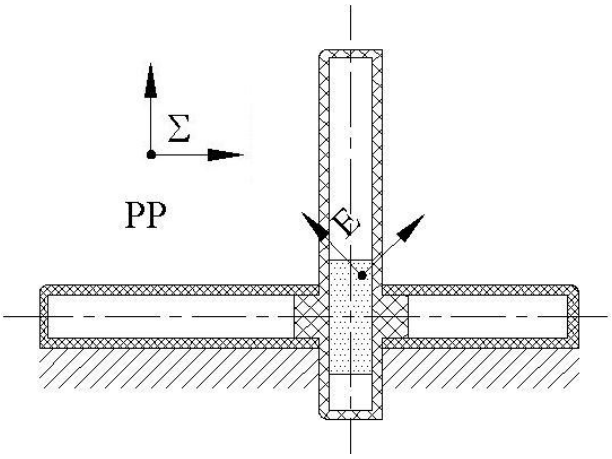

Figure 3.3: A PP dyad.

a plane given by $X_3 = \tan\frac{\theta}{2}$.

3.2.1 RR Dyad Circular Constraints

The moving revolute joint in an RR-dyad is constrained to move on a fixed circle. Meanwhile, a second rigid body can rotate about that moving revolute joint if that is the only attachment point. These two degrees of freedom correspond to a two parameter hyperboloid of one sheet in the image space. An example of this type of hyperboloid is shown in Figure 3.4. For the particular type of hyperboloid defined by the RR dyad, the trace of the surface is a circle in planes parallel to $X_3 = 0$ [42]. The circle corresponding to a particular value of X_3 represents all possible coupler displacements at the fixed angle proportionate to the particular value of X_3. The coefficients defining the constraints are then

$$\begin{aligned} K_0 &= 1, \\ K_1 &= -X_c, \\ K_2 &= -Y_c, \\ K_3 &= K_1^2 + K_2^2 - r^2, \end{aligned} \tag{3.11}$$

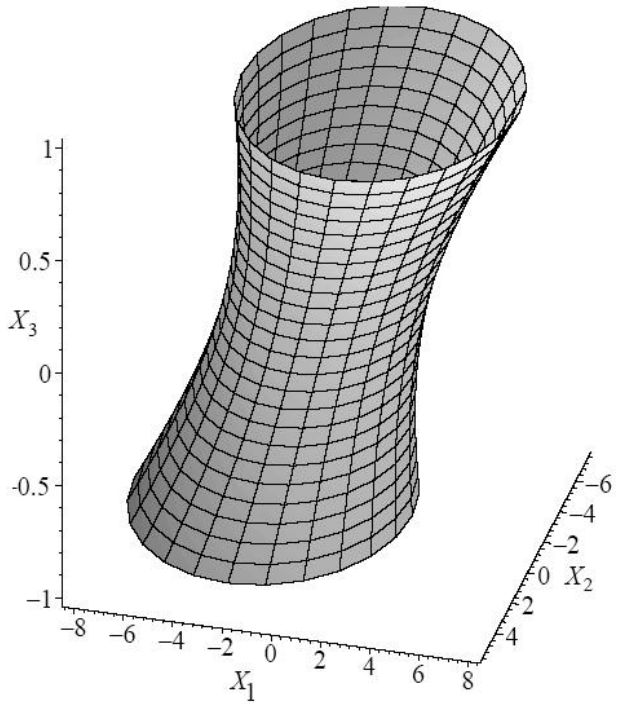

Figure 3.4: A two parameter hyperboloid of one sheet.

where (X_c, Y_c) are the Cartesian coordinates of the fixed circle centre and r is the circle radius. Together with x and y, which define the position of the moving revolute joint in coordinate frame E, the K_i, x, and y define the shape of the constraint surface for the RR dyad.

3.2.2 PR Dyad Linear Constraints

Linear constraints result when PR and RP dyads are employed. The linear shape coefficients are defined as

$$[K_0 : K_1 : K_2 : K_3] = [0 : \tfrac{1}{2}L_1 : \tfrac{1}{2}L_2 : L_3], \tag{3.12}$$

where the L_i are line coordinates obtained by Grassmann expansion of the determinant of any two distinct points on the line [44].

The direction of the line is constant, defined by the angle ϑ it makes with the X-axis of Σ, indicated by ϑ_Σ. The location of points on the line in Σ are given by the coordinates F_Σ. The equation of the line in Σ for a given PR-dyad is obtained from the Grassmann expansion:

$$\begin{vmatrix} X & Y & Z \\ F_{X/\Sigma} & F_{Y/\Sigma} & F_{Z/\Sigma} \\ \cos\vartheta_\Sigma & \sin\vartheta_\Sigma & 0 \end{vmatrix} = 0, \tag{3.13}$$

where $(F_{X/\Sigma} : F_{Y/\Sigma} : F_{Z/\Sigma})$ represents the homogeneous point coordinates $(X : Y : Z)$ of any convenient fixed point on the line in Σ, and ϑ_Σ represents the angle ϑ the line makes with respect to the positive X-axis of Σ. Using Equation (3.12) and Equation (3.13) the parameters defining the PR dyad are

$$\begin{aligned} K_0 &= 0, \\ K_1 &= -\frac{F_{Z/\Sigma}}{2}\sin\vartheta_\Sigma, \\ K_2 &= \frac{F_{Z/\Sigma}}{2}\cos\vartheta_\Sigma, \\ K_3 &= F_{X/\Sigma}\sin\vartheta_\Sigma - F_{Y/\Sigma}\cos\vartheta_\Sigma. \end{aligned} \tag{3.14}$$

Once a point on the line is known, together with its angle ϑ, we obtain the line coefficients $[K_0 : K_1 : K_2 : K_3]$. These coefficients, together with x and y, define the constraint surface for a PR dyad by substituting them into Equation (3.10). The surface is a hyperbolic paraboloid. This particular hyperbolic paraboloid defined by the PR dyad has one regulus ruled by skew lines that are all parallel to $X_3 = 0$ [42]. An example is shown in Figure 3.5.

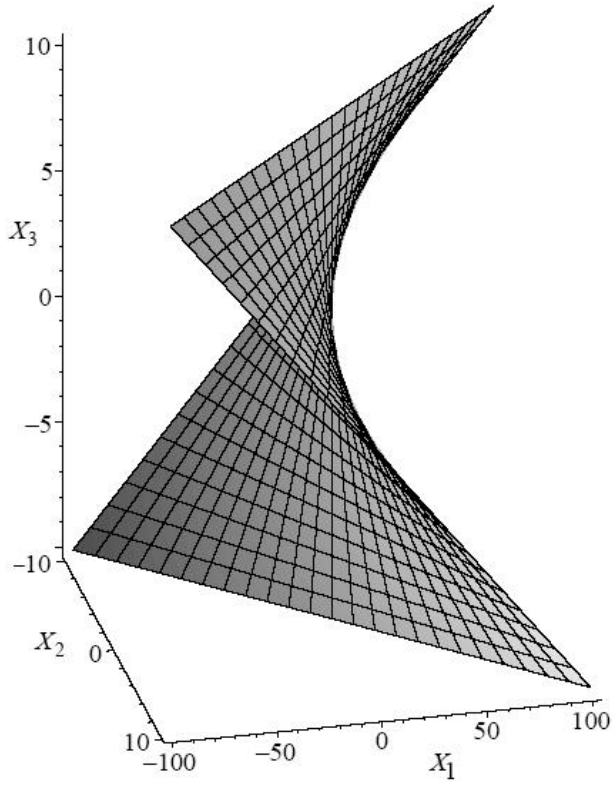

Figure 3.5: A hyperbolic paraboloid.

3.2.3 RP Dyad Linear Constraints

Since the RP dyad is simply the kinematic inverse of the PR dyad, the formulation is similar. However, instead of a fixed point in E moving on a fixed line in Σ, a fixed line in E now moves on a fixed point in Σ. Equation (3.13) then becomes

$$\begin{vmatrix} x & y & z \\ M_{x/E} & M_{y/E} & M_{z/E} \\ \cos\vartheta_E & \sin\vartheta_E & 0 \end{vmatrix} = 0, \tag{3.15}$$

where M_E represents the homogeneous coordinates $(x : y : z)$ of any convenient fixed point on the line that is fixed in E. The K_i are then

$$\begin{aligned} K_0 &= 0, \\ K_1 &= -\frac{M_{z/E}}{2}\sin\vartheta_E, \\ K_2 &= \frac{M_{z/E}}{2}\cos\vartheta_E, \\ K_3 &= M_{x/E}\sin\vartheta_E - M_{y/E}\cos\vartheta_E. \end{aligned} \tag{3.16}$$

RP dyads also yield hyperbolic paraboloids in the image space.

3.2.4 PP Dyad Linear Constraints

The PP dyad gives a trivial linear constraint. Since this type of dyad permits no change in orientation, points on the distal rigid body are constrained to move on curvilinear paths. Thus the constraint imposed by the dyad is the degenerate quadric

$$X_3 = \tan\frac{\theta}{2}. \tag{3.17}$$

3.3 Kinematic Synthesis Using Kinematic Mapping

Every pose of E determines a point, $(X_1 : X_2 : X_3 : X_4)$, in the image space. A planar motion, composed of a continuous set of poses, will define a curve of points in the image space. If this motion can be reproduced by a planar four-bar mechanism, the corresponding curve in the image space will be coincident with the curve of intersection of two constraint quadric surfaces. These two constraint surfaces completely define the two dyads that comprise the mechanism.

In general, nine points are required to specify a quadric surface. However, the special nature of the constraint surfaces corresponding to RR, PR, and RP dyads constrain the surfaces such that only five points are needed [36]. If five poses are defined, there may be zero, two, or four unique constraint surfaces that that contain those points [3]. Pairing dyads to form solutions results in the possibility of there being zero, one, or six distinct planar four-bar mechanisms that can guide a rigid body exactly through those five defined poses. Determining constraint surfaces that contain the five poses is acheived by solving the corresponding five equations (3.10) for the parameters that define the constraint surface. In other words, the solution is obtained by solving for sets of K_i, x, and y that simultaneously satisfy the set of five equations resulting from the five sets of image space points X_i. The number of distinct sets of solutions to those parameters is the number of unique dyads that, when paired, form a mechanism that can guide a rigid body exactly through the specified five poses.

One may notice that, although only five points are needed to construct a constraint surface, there are six parameters in total that define it. But since K_0 may only be equal to 1 or 0, it does not constitute a full degree of freedom. However, the value of K_0 is the only difference in the mathematical form of RR and PR dyads. This property is advantageous for integrating type with dimensional synthesis.

The approach then is to leave K_0 as an unspecified variable homogenizing coordinate and solve the synthesis equations in terms of it. If the K_i parameters become disproportionately large compared to the image space coordinates, the resulting mechanism will then have extremely large link lengths. The conclusion then is that a PR dyad would be better suited, and so the parameters are re-computed using the line coordinate definitions in Equation (3.14). RP dyads, being kinematic inverses of PR dyads, can be determined using similar means. Otherwise, if the K_i are of reasonable order, the circle coordinate definitions given in Equation (3.11) are used to reveal an RR dyad [1].

For n poses, where $n > 5$, an exact solution, in general, does not exist. The problem then turns to approximate synthesis, where the intent is to find a planar mechanism that minimizes the error in attaining the desired poses. In kinematic mapping terms, the intent is to find constraint surfaces that best fit curves defined by n points in the image space. The optimal solution is the pairing of the two constraint surfaces that best fit the curve, and the motion that is generated is characterized by the curve of intersection of those two surfaces. The two dyads corresponding to those constraint surfaces then make up the mechanism. Unlike the Burmester problem, where the number of solutions may be zero, one, or six, the best solution to the approximate synthesis problem is unique, depending on the optimization criteria.

The solution to the approximate synthesis problem is achieved by the simultaneous minimization in a least squares sense of a system of n equations defined by Equation (3.10), with each pose or image space point giving an equation. Equation (3.10) appears to be highly nonlinear, with squared and bilinear terms thoughout. At first glance, the only solution appears to be nonlinear least squares optimization. However, attempts were made to manipulate Equation (3.10) such that linear techniques could be applied. Singular value decomposition is an extremely powerful technique applied to linear systems of homogeneous equations. Limited success was achieved in applying this technique to

approximate kinematic synthesis [1].

3.4 Singular Value Decomposition

Singular value decomposition (SVD) [45] decomposes any given $m \times n$ matrix $\mathbf{C}$ into the product of three matrix factors such that

$$\mathbf{C}_{m\times n} = \mathbf{U}_{m\times m}\mathbf{S}_{m\times n}\mathbf{V}^T_{n\times n}, \tag{3.18}$$

where $\mathbf{U}$ and $\mathbf{V}$ are orthogonal, and $\mathbf{S}$ is a rectangular matrix whose only non-zero elements are on the diagonal of the upper $n\times n$ sub-matrix. These diagonal elements are the singular values of $\mathbf{C}$ arranged in descending order, lower bounded by zero [46].

For the application of kinematic synthesis using kinematic mapping, an "economy size" version of SVD is used instead, which produces only the first n columns of $\mathbf{U}$ and n rows of $\mathbf{S}$ [47]. This form of SVD is

$$\mathbf{C}_{m\times n} = \mathbf{U}_{m\times n}\mathbf{S}_{n\times n}\mathbf{V}^T_{n\times n}. \tag{3.19}$$

SVD constructs orthonormal bases spanning the range of $\mathbf{C}$ in $\mathbf{U}$ and the nullspace of $\mathbf{C}$ in $\mathbf{V}$. This can be used to great advantage for any set of homogeneous linear equations of the form $\mathbf{CK} = \mathbf{0}$, where $\mathbf{C}$ must be rank deficient in order for non-trivial $\mathbf{K}$. If $\mathbf{C}$ is rank deficient, then the last $n-\text{rank}(\mathbf{C})$ singular values of $\mathbf{C}$ are zero. Furthermore, the corresponding columns of $\mathbf{V}$ span the nullspace of $\mathbf{C}$. As such, any of these columns is a non-trivial solution to $\mathbf{CK} = \mathbf{0}$. For overconstrained systems, where the $m \times n$ matrix $\mathbf{C}$ has $m > n$, in general no non-trivial exact solution exists. In this case, the optimal approximate solution in a least squares sense is found to be the last column of $\mathbf{V}$ corresponding to the smallest singular value of $\mathbf{C}$.

3.5 Kinematic Synthesis Using Kinematic Mapping and Singular Value Decomposition

In order to apply SVD to kinematic synthesis using kinematic mapping, Equation (3.10) must first be expressed in linear terms with respect to the unknown parameters. The known parameters, which are the sets of X_i that define the points in the image space, will make up $\mathbf{C}$. The unknown parameters, K_i and x and y will populate the vector $\mathbf{K}$. Algebraically manipulating Equation (3.10) towards this end yields

$$\mathbf{CK} = \begin{bmatrix} \left[\frac{1}{4}\left(\mathbf{X_3^2}+\mathbf{1}\right)\right] \\ [\mathbf{X_2}-\mathbf{X_1X_3}] \\ \left[\frac{1}{4}\left(\mathbf{X_3^2}+\mathbf{1}\right)\right] \\ [\mathbf{X_1}+\mathbf{X_2X_3}] \\ [\mathbf{X_2^2}+\mathbf{X_1^2}] \\ \left[\frac{1}{2}\left(\mathbf{1}-\mathbf{X_3^2}\right)\right] \\ [-\mathbf{X_3}] \\ [\mathbf{X_1X_3}+\mathbf{X_2}] \\ [\mathbf{X_3}] \\ \left[\frac{1}{2}\left(\mathbf{1}-\mathbf{X_3^2}\right)\right] \\ [-\mathbf{X_1}+\mathbf{X_2X_3}] \\ \left[\frac{1}{4}\left(\mathbf{X_3^2}+\mathbf{1}\right)\right] \end{bmatrix}^T \begin{bmatrix} x^2K_0 \\ xK_0 \\ y^2K_0 \\ K_0 \\ xK_1 \\ yK_1 \\ K_1 \\ xK_2 \\ yK_2 \\ K_2 \\ K_3 \end{bmatrix} = [\mathbf{0}]_{n\times 1}\,. \tag{3.20}$$

With each component of $\mathbf{C}$ listed in Equation (3.20) being an n dimensional column vector, $\mathbf{C}$ becomes an $n \times 12$ matrix. Upon investigation of Equation (3.20), it becomes clear that this formulation has some problems. First of all, the unknown vector $\mathbf{K}$, which has twelve elements, overdetermines the unknowns, of which there are only six, including K_0. Similarly, $\mathbf{C}$ being twelve columns wide gives too much room for rank deficiency.

Theoretically, since only five points are needed to define a constraint surface, $\mathbf{C}$ should be at most six columns wide. Five points making $\mathbf{C}$ an $n \times 6$ matrix would guarantee a nullity of one, thus the correct dimensions to find a solution to one dyad. With twelve columns, applying SVD to $\mathbf{C}$ would erroneously determine an exact solution for a constraint surface with as many as eleven image space points, more than twice the exact number actually required. In reality, eleven image space points would overconstrain the system such that no exact solution could be found.

Further algebraic manipulation is necessary to bring the system of equations to a more useful form, such as Equation (3.21):

$$\mathbf{CK} = \begin{bmatrix} [\mathbf{X_1^2} + \mathbf{X_2^2}] \\ [\mathbf{X_2} + \mathbf{X_1 X_3}] \\ [\mathbf{X_2 X_3} - \mathbf{X_1}] \\ [\mathbf{X_2} - \mathbf{X_1 X_3}] \\ [-\mathbf{X_1} - \mathbf{X_2 X_3}] \\ \left[\frac{1}{4}\left(\mathbf{1} + \mathbf{X_3^2}\right)\right] \\ \left[\frac{1}{2}\left(\mathbf{1} - \mathbf{X_3^2}\right)\right] \\ [\mathbf{X_3}] \end{bmatrix}^T \begin{bmatrix} K_0 \\ K_1 \\ K_2 \\ K_0 x \\ K_0 y \\ K_0\left(x^2 + y^2\right) + K_3 \\ K_1 x + K_2 y \\ K_2 x - K_1 y \end{bmatrix} = [\mathbf{0}]_{n \times 1}\,. \tag{3.21}$$

Although the number of columns is reduced by four, an eight column matrix with an eight parameter vector of unknowns is still not the correct dimension to solve the problem correctly. In order to further pursue a solution using this method, the problem must be split into separate components: the search for RR, PR, and RP dyads individually.

3.5.1 *RR* Dyads

For an *RR* dyad, $K_0 = 1$. This result simplifies Equation (3.21), but not as much as is needed, since no parameters or columns are eliminated. The result is

$$\mathbf{CK} = \begin{bmatrix} [\mathbf{X_1^2 + X_2^2}] \\ [\mathbf{X_2 + X_1 X_3}] \\ [\mathbf{X_2 X_3 - X_1}] \\ [\mathbf{X_2 - X_1 X_3}] \\ [\mathbf{-X_1 - X_2 X_3}] \\ \left[\frac{1}{4}\left(\mathbf{1 + X_3^2}\right)\right] \\ \left[\frac{1}{2}\left(\mathbf{1 - X_3^2}\right)\right] \\ [\mathbf{X_3}] \end{bmatrix}^T \begin{bmatrix} 1 \\ K_1 \\ K_2 \\ x \\ y \\ x^2 + y^2 + K_3 \\ K_1 x + K_2 y \\ K_2 x - K_1 y \end{bmatrix} = [\mathbf{0}]_{n \times 1} . \tag{3.22}$$

Since no parameters can be eliminated, the matrix equation remains in a form unusable by SVD. Unfortunately, due to the generality of *RR* dyads, the problem cannot be formulated to make use of linear techniques. See Chapter 4. The solution at this point may only be pursued using simultaneous optimization of nonlinear systems of equations. In general, *RR* dyads cannot be synthesized using this linear technique. Only in special cases can this technique be used to synthesize *RR* dyads. For an example, see Section 3.6.3.

3.5.2 *PR* Dyads

For a *PR* dyad, setting $K_0 = 0$ leaves only five unkowns. Also, with $K_0 = 0$, Equation (3.21) is simplified considerably. The first, fourth, and fifth elements of the unknown parameter vector become zero, leaving only five parameters. The corresponding columns of **C** also become zero, since they are multiplied by the parameters that are now zero.

This leaves Equation (3.23).

$$\mathbf{CK} = \begin{bmatrix} [\mathbf{X_2} + \mathbf{X_1}\mathbf{X_3}] \\ [\mathbf{X_2}\mathbf{X_3} - \mathbf{X_1}] \\ \left[\frac{1}{4}\left(\mathbf{1} + \mathbf{X_3^2}\right)\right] \\ \left[\frac{1}{2}\left(\mathbf{1} - \mathbf{X_3^2}\right)\right] \\ [\mathbf{X_3}] \end{bmatrix}^T \begin{bmatrix} K_1 \\ K_2 \\ K_3 \\ K_1 x + K_2 y \\ K_2 x - K_1 y \end{bmatrix} = [\mathbf{0}]_{n\times 1}\,. \tag{3.23}$$

It is apparent that this is the form necessary for finding a solution. With a five parameter unknown vector, it matches the number of unknowns that need to be solved for. Therefore, five points in the image space will determine the solution exactly, as required by Burmester theory. For n points greater than five, the system of equations is overconstrained, and one proceeds as detailed in Section 3.4.

3.5.3 *RP* Dyads

Analogous to *PR* dyads, the solution for *RP* dyads is similar. Once again, $K_0 = 0$. However, due to the inverse in the kinematic constraint, the lower signs in Equation (3.10) are used, and x and y are replaced with X and Y. The resulting formulation in the same form as Equation (3.23) is then expressed by Equation (3.24).

$$\mathbf{CK} = \begin{bmatrix} [-\mathbf{X_2} + \mathbf{X_1}\mathbf{X_3}] \\ [\mathbf{X_2}\mathbf{X_3} + \mathbf{X_1}] \\ \left[\frac{1}{4}\left(\mathbf{1} + \mathbf{X_3^2}\right)\right] \\ \left[\frac{1}{2}\left(\mathbf{1} - \mathbf{X_3^2}\right)\right] \\ [-\mathbf{X_3}] \end{bmatrix}^T \begin{bmatrix} K_1 \\ K_2 \\ K_3 \\ K_1 X + K_2 Y \\ K_2 X - K_1 Y \end{bmatrix} = [\mathbf{0}]_{n\times 1}\,. \tag{3.24}$$

Examples of kinematic synthesis using kinematic mapping are given in the next section.

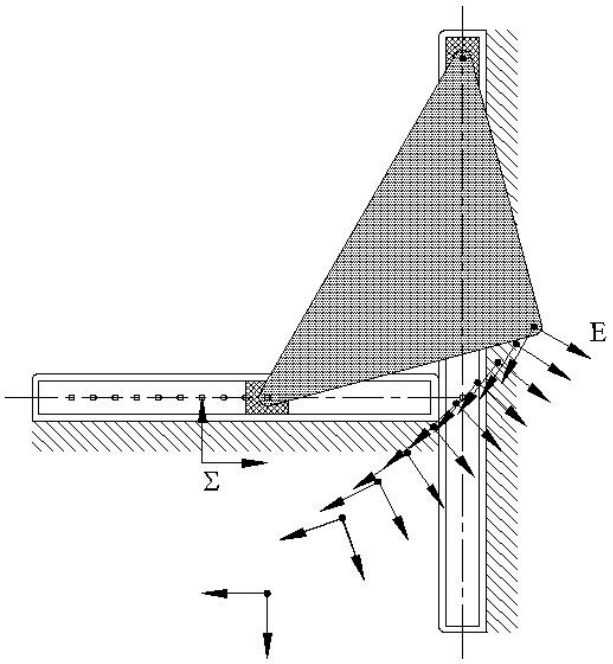

Figure 3.6: The $PRRP$ mechanism.

3.6 Kinematic Mapping Examples

These examples detail the procedure in determining the dimensions of dyads which, when paired, will form a mechanism that best approximates the specified poses. The first example attempts to find two PR dyads to form a $PRRP$ mechanism. The second example attempts to find two RP dyads to form an $RPPR$ mechanism. The third example attempts to find an RR dyad and PR dyad to form a $PRRR$ mechanism. These examples will illustrate the advantages and limitations of this method.

3.6.1 PR Dyads

This first example illustrates the process for determining PR dyads. Ten poses were used in this example. The mechanism used to generate the ten poses is shown in Figure 3.6, while the poses are given in Table 3.1. The rigid body attachment points in E are (-3,-3) and (3,-3).

Pose	x	y	θ
1	5.0981	2.0981	-120.0000
2	4.8278	1.8278	-123.7490
3	4.5413	1.5413	-127.6699
4	4.2361	1.2361	-131.8103
5	3.9083	0.9083	-136.2383
6	3.5523	0.5523	-141.0576
7	3.1583	0.1583	-146.4427
8	2.7077	-0.2923	-152.7340
9	2.1527	-0.8473	-160.8119
10	1.0000	-2.0000	-180.0000

Table 3.1: Poses of the $PRRP$ mechanism.

Parameter	Value
K_1	0.1622
K_2	-0.1622
K_3	-0.9733
$K_1x + K_2y$	0.0000
$K_2x - K_1y$	0.0000

Table 3.2: Vector **K** corresponding to the smallest singular value of **C**.

Using Equation (3.9), the poses are mapped into the image space, defined by X_i. Those image space points are then substituted into Equation (3.23) to form **C**. SVD is then applied to the system of equations yielding a solution. The smallest singular value of **C** is 7.4643×10^{-15}. The vector **K** corresponding to this singular value is listed in Table 3.2.

From these parameters, it is calculated that (x, y) is (0,0), which defines the attachment point of the dyad to the rigid body. Having x, y, and K_i, one dyad is determined. This dyad defines a revolute joint attached to the rigid body at the coordinates (0,0) in frame E, forced to move on the prismatic joint defined by the line $Y = X - 3$ in frame Σ.

Although this dyad does facilitate the motion defined by the poses given in Table 3.1, the determined dyad is not one of the dyads in the mechanism used to generate the poses. Unfortunately, the next smallest singular value of **C** is 0.6983. If it were instead

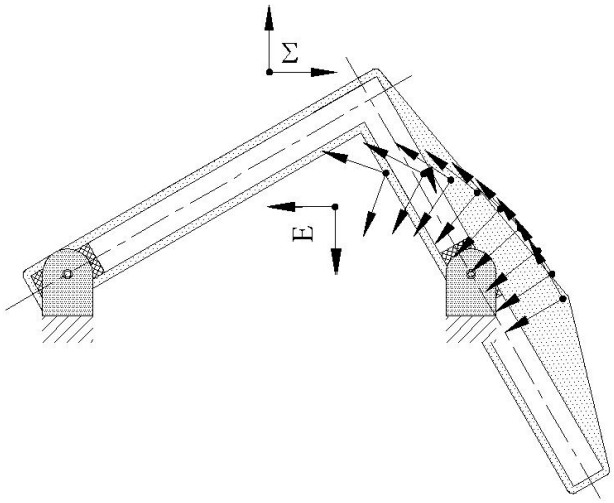

Figure 3.7: The $RPPR$ mechanism.

close to zero, a second dyad corresponding to that singular value could be solved for. However, since this is not the case, there are no more possible solutions to be found using this method. Only one dyad could be identified out of the two necessary for a complete solution. Moreover, the dyad identified does not match either of the dyads in the generating mechanism. For this example, the intended mechanism could not be identified using this method.

3.6.2 RP Dyads

This second example illustrates the process for determining RP dyads. Ten poses were used in this example. The mechanism used to generate the ten poses is shown in Figure 3.7. The poses are given in Table 3.3.

Using Equation (3.9), the poses are mapped into the image space, defined by X_i. Those image space points are then substituted into Equation (3.24) to form $\mathbf{C}$. SVD is then applied to the equation to yield the solution. The smallest singular value of $\mathbf{C}$ is 3.4777×10^{-14}. The vector $\mathbf{K}$ corresponding to this singular value is given in Table 3.4.

Notice that these parameters are identical to those found in the previous example.

Pose	x	y	θ
1	4.3660	-3.3660	120.0000
2	4.2018	-2.9988	123.7490
3	3.9952	-2.6527	127.6699
4	3.7454	-2.3333	131.8103
5	3.4509	-2.0472	136.2383
6	3.1100	-1.8032	141.0576
7	2.7194	-1.6139	146.4427
8	2.2729	-1.5003	152.7340
9	1.7546	-1.5078	160.8119
10	1.0000	-2.0000	180.0000

Table 3.3: Poses of the $RPRP$ mechanism.

Parameter	Value
K_1	0.1622
K_2	-0.1622
K_3	-0.9733
$K_1X + K_2Y$	0.0000
$K_2X - K_1Y$	0.0000

Table 3.4: Vector **K** corresponding to the smallest singular value of **C**.

From these parameters, it is calculated that (X, Y) is (0,0), which defines the revolute centre in frame Σ. Having X, Y, and K_i, one dyad is determined. This dyad defines a prismatic joint defined by the line $y = x - 3$ in frame E, forced to move on the revolute joint at the coordinates (0,0) in frame Σ. As in the previous example, this dyad facilitates the motion defined by the poses given in Table 3.3. However, the determined dyad is not one of the dyads in the mechanism used to generate the poses, as was the case in the previous example.

The similarity of the dyad determined for this example and the previous example can be explained by the fact that the two generating mechanisms used for the examples are kinematic inversions of one another. The only difference in the two examples is that the moving frame E and fixed frame Σ are switched. Thus the PR dyads in the previous example became RP dyads in this example. With this characteristic established, it is

now evident that the same dyad has been determined for both examples. In the previous example, the determined dyad was a revolute joint at (0,0) in frame E, forced to move on the prismatic joint defined by the line $Y = X - 3$ in frame Σ. In this example, the determined dyad is kinematically inverted.

The dyads used to generate the poses can not be found for this example. Since the poses used were exact poses from a known generating mechanism, it is expected that the singular values corresponding to a least squares solution would be zero, up to the computer precision. The next smallest singular value of $\mathbf{C}$ is 0.6983, which is much too large to be considered as a result of round-off error from numerical computation. Therefore, this singular value does not correspond to a least squares solution. Like the previous example, only one dyad was determined out of the two necessary for a complete solution. Furthermore, the determined dyad does not match either of the two dyads in the generating mechanism.

3.6.3 *RR* Dyads

The final example of this chapter illustrates the process for determining RR dyads, taken from [1]. In Section 3.5.1, it was concluded that, in general, RR dyads could not be synthesized using this method. This example gives insight into the conditions in which RR dyads *can* be synthesized.

Twenty poses were used in this example. The mechanism used to generate the ten poses is shown in Figure 3.8, while the poses are given in Table 3.5.

First, the PR dyad is determined in the usual way. Using Equation (3.9), the poses are mapped into the image space, defined by X_i. Those image space points are then substituted into Equation (3.23) to form $\mathbf{C}$. SVD is then applied to the system of equations yielding a solution. The smallest singular value of $\mathbf{C}$ is 2.6130×10^{-16}. The vector $\mathbf{K}$ corresponding to this singular value is listed in Table 3.6.

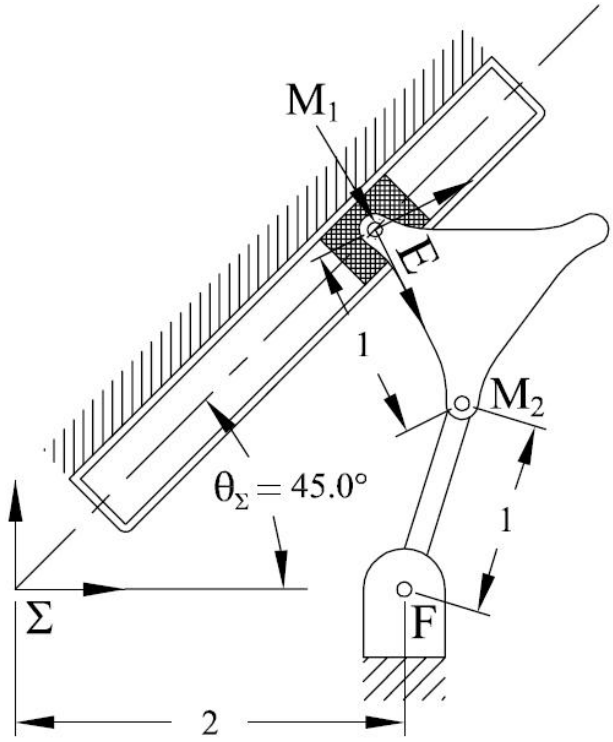

Figure 3.8: The $PRRR$ mechanism [2].

From these parameters, it is calculated that (x, y) is (0,0), which defines the attachment point of the dyad to the rigid body. Having x, y, and K_i, one dyad is determined. This dyad defines a revolute joint attached to the rigid body at the coordinates (0,0) in frame E, forced to move on the prismatic joint defined by the line $Y = X$ in frame Σ. This dyad matches the PR dyad of the generating mechanism.

In order to identify the RR dyad, the image space points are substituted into Equation (3.22) to form $\mathbf{C}$. However, since it is known from Section 3.5.1 that this matrix equation will not yield a solution, simplifications must be made to Equation (3.22). Adding the

Pose	x	y	θ
1	1.0956	1.0956	5.7248
2	1.1005	1.1005	6.0256
3	1.1058	1.1058	6.3597
4	1.1117	1.1117	6.7329
5	1.1184	1.1184	7.1527
6	1.1259	1.1259	7.6281
7	1.1344	1.1344	8.1712
8	1.1441	1.1441	8.7974
9	1.1554	1.1554	9.5273
10	1.1687	1.1687	10.3889
11	1.1844	1.1844	11.4212
12	1.2034	1.2034	12.6804
13	1.2268	1.2268	14.2500
14	1.2563	1.2563	16.2602
15	1.2949	1.2949	18.9246
16	1.3474	1.3474	22.6199
17	1.4229	1.4229	28.0725
18	1.5403	1.5403	36.8699
19	1.7403	1.7403	53.1301
20	2.0000	2.0000	90.0000

Table 3.5: Poses of the $PRRP$ mechanism [2].

second and third columns of Equation (3.22) results in the equation

$$\mathbf{CK} = \begin{bmatrix} [\mathbf{X_1^2} + \mathbf{X_2^2}] \\ [\mathbf{X_2} + \mathbf{X_1X_3} + \mathbf{X_2X_3} - \mathbf{X_1}] \\ [\mathbf{X_2} - \mathbf{X_1X_3}] \\ [-\mathbf{X_1} - \mathbf{X_2X_3}] \\ \left[\frac{1}{4}\left(\mathbf{1} + \mathbf{X_3^2}\right)\right] \\ \left[\frac{1}{2}\left(\mathbf{1} - \mathbf{X_3^2}\right)\right] \\ [\mathbf{X_3}] \end{bmatrix}^T \begin{bmatrix} 1 \\ K_1 + K_2 \\ x \\ y \\ x^2 + y^2 + K_3 \\ K_1x + K_2y \\ K_2x - K_1y \end{bmatrix} = [\mathbf{0}]_{n\times 1}\,. \tag{3.25}$$

This addition of columns is possible when $\frac{X_1 - X_2X_3}{X_1X_3 + X_2}$ has the same value for the entire data set. This occurs only when the PR dyad has parameters $K_3 = x = y = 0$. As shown

Parameter	Value
K_1	0.7071
K_2	-0.7071
K_3	1.0000
$K_1x + K_2y$	0.0000
$K_2x - K_1y$	0.0000

Table 3.6: Vector **K** corresponding to the smallest singular value of **C**.

Parameter	Value
$K_1 + K_2$	-1.0000
x	1.0000
y	0.0000
$x^2 + y^2 + K_3$	4.0000
$K_1x + K_2y$	-2.0000
$K_2x - K_1y$0.0000	

Table 3.7: Vector **K** corresponding to the smallest singular value of **C**.

in Table 3.5, this is the case. Applying SVD to Equation (3.25) yields the parameter vector as given in Table 3.7. From Table 3.6, the RR dyad geometry is extracted as the point $(x, y) = (1, 0)$ in moving frame E constrained to move on the fixed circle having centre $(2, 0)$ and link length of 1. This dyad also matches the dyad from the generating mechanism, completing the solution.

Unfortunately, the linear techniques applied to kinematic mapping for kinematic synthesis have yet to produce consistently successful results. The main disadvantage to this procedure is that it cannot in general identify RR dyads, which are the most general in planar kinematics. RR dyads can only be identified in special cases, such as the example given above. Also, these examples have shown that not all PR and RP dyads can be identified. In the next section, a procedure is presented which finally solves the integrated type and approximate dimensional synthesis problem for rigid-body guidance.

Chapter 4

A Complete and General Solution

In this chapter, a method is proposed for the first time that robustly combines geometric and numerical methods to combine type and approximate dimensional synthesis of planar four-bar mechanisms for rigid body guidance. The developed algorithm sizes link lengths, locates joint axes, and decides between all four types of dyads that, when combined, guides a rigid body through the best approximation of n specified positions and orientations in a least squares sense, where $n \geq 5$. In this chapter, the kinematic theory pertaining to this method is first summarized. Secondly, the method of correlating points of interest in both reference frames is detailed. Numerical considerations follow, which introduce practical methods for implementing the theory. Finally, the procedures to find RP and PP dyads are discussed. As they are both special cases, they require special attention.

4.1 Kinematic Theory Summary

The homogeneous transformation that maps a point from the moving frame E to the fixed frame Σ is reprinted below from Equation (3.1) for convenience.

$$\begin{bmatrix} X \\ Y \\ Z \end{bmatrix} = \begin{bmatrix} \cos\theta & -\sin\theta & a \\ \sin\theta & \cos\theta & b \\ 0 & 0 & 1 \end{bmatrix} \begin{bmatrix} x \\ y \\ z \end{bmatrix}.$$

Note that this transformation is determined by the relative displacement of the two coordinate frames. For rigid body guidance, each pose is defined by the position and orientation of E with respect to Σ, as represented by (a, b, θ). Dyads are connected through the coupler link at the coupler attchment points M_1 and M_2.

The equation of a line or circle given in Equation (3.7) can be expressed in matrix form as

$$\mathbf{CK} = \begin{bmatrix} X^2 + Y^2 & 2X & 2Y & 1 \end{bmatrix} \begin{bmatrix} K_0 \\ K_1 \\ K_2 \\ K_3 \end{bmatrix} = 0,$$

where X and Y are points on a circle or line, and the K_i define the geometry. For a circle,

$$\begin{aligned} K_0 &= 1, \\ K_1 &= -X_c, \\ K_2 &= -Y_c, \\ K_3 &= K_1^2 + K_2^2 - r^2, \end{aligned}$$

as was given in Section 3.2.1 in Equation (3.11). (X_c, Y_c) is the circle centre in Σ and r is

the circle radius. For a line,

$$\begin{aligned} K_0 &= 0, \\ K_1 &= -\frac{F_{Z/\Sigma}}{2}\sin\vartheta_\Sigma, \\ K_2 &= \frac{F_{Z/\Sigma}}{2}\cos\vartheta_\Sigma, \\ K_3 &= F_{X/\Sigma}\sin\vartheta_\Sigma - F_{Y/\Sigma}\cos\vartheta_\Sigma, \end{aligned}$$

as was also given in Section 3.2.1 in Equation (3.14). $(F_X : F_Y : F_Z)$ are homogeneous point coordinates on the line that make an angle ϑ with the positive X-axis in Σ. By relating the position of the two rigid body attachment points M_1 and M_2 in both reference frames E and Σ, the following method solves the planar kinematic synthesis problem.

4.2 Reference Frame Correlation

This method determines the solution from the application of two important relations:

1. Points M_1 and M_2 move on circles or lines in Σ,

2. Points M_1 and M_2 have constant coordinates in E.

Let (x, y) be the coordinates of one of the rigid body attachment points to a dyad expressed in E, and (X, Y) be the coordinates of the same point expressed in Σ. Carrying out the matrix multiplication in Equation (3.1) yields

$$\begin{aligned} X &= x\cos\theta - y\sin\theta + az, \\ Y &= x\sin\theta + y\cos\theta + bz, \\ Z &= z. \end{aligned} \tag{4.1}$$

Ignoring displacements at infinity, it is reasonable to set $z = 1$, resulting in

$$\begin{aligned} X &= x\cos\theta - y\sin\theta + a, \\ Y &= x\sin\theta + y\cos\theta + b, \\ Z &= 1. \end{aligned} \tag{4.2}$$

Constraining (X, Y) to move on a circle or line, Equation (4.2) is substituted into Equation (3.7), yielding

$$\mathbf{CK} = \begin{bmatrix} (x\cos\theta - y\sin\theta + a)^2 + (x\sin\theta + y\cos\theta + b)^2 \\ 2\,(x\cos\theta - y\sin\theta + a) \\ 2\,(x\sin\theta + y\cos\theta + b) \\ 1 \end{bmatrix}^T \begin{bmatrix} K_0 \\ K_1 \\ K_2 \\ K_3 \end{bmatrix} = 0. \tag{4.3}$$

For n poses of E, (X, Y) become arrays of n points. The parameters a, b, and θ in $\mathbf{C}$ then become n dimensional vectors, making $\mathbf{C}$ an $n \times 4$ matrix. The parameters x and y do not become n dimensional vectors because their values are constant in E. The n-dimensional vector parameters $\mathbf{a}$, $\mathbf{b}$, and $\boldsymbol{\theta}$ in $\mathbf{C}$ are all defined, as they constitute the poses of E with respect to Σ. This yields

$$\mathbf{CK} = \begin{bmatrix} \left[(x\cos\boldsymbol{\theta} - y\sin\boldsymbol{\theta} + \mathbf{a})^2 + (x\sin\boldsymbol{\theta} + y\cos\boldsymbol{\theta} + \mathbf{b})^2\right] \\ [(x\cos\boldsymbol{\theta} - y\sin\boldsymbol{\theta} + \mathbf{a})] \\ [(x\sin\boldsymbol{\theta} + y\cos\boldsymbol{\theta} + \mathbf{b})] \\ [\mathbf{1}] \end{bmatrix}^T \begin{bmatrix} K_0 \\ K_1 \\ K_2 \\ K_3 \end{bmatrix} = [\mathbf{0}]_{n\times 1}\,. \tag{4.4}$$

The only parameters left to find in $\mathbf{C}$ are then x and y. Determining the x and y that satisfies Equation (4.4) will solve the problem. Once x and y are obtained, $\mathbf{C}$ is then fully determined, which allows the vector $\mathbf{K}$ defining the K_i to be solved for using singular value

decomposition. Please refer to Section 3.4 for more details on singular value decomposition (SVD).

The problem is now a two dimensional search for x and y. However, at least two dyads are required to form a planar mechanism solution. This implies that there must be at least two sets of values for (x, y) for a complete solution to exist. x and y are found such that they satisfy Equation (4.4). For equations of the form $\mathbf{CK} = \mathbf{0}$, if $\mathbf{C}$ is not singular, the only $\mathbf{K}$ in existance that satisfies the equation is the zero vector. In order for $\mathbf{K}$ to be non-trivial, $\mathbf{C}$ must be singular [48]. The task then becomes to find values for x and y that makes $\mathbf{C}$ become singular, or, failing that, the most ill-conditioned.

4.3 Numerical Considerations

The conditioning of a matrix is measured by the ratio of the largest and smallest singular values of the matrix, which is called the condition number κ [45].

$$\kappa \equiv \frac{\sigma_{MAX}}{\sigma_{MIN}}, 1 \leq \kappa \leq \infty. \tag{4.5}$$

A more convenient number to use is the inverse of the condition number γ

$$\gamma \equiv \frac{1}{\kappa}, 0 \leq \gamma \leq 1, \tag{4.6}$$

because it is bounded both from above and below. A well conditioned matrix has $\gamma \approx 1$, while an ill-conditioned matrix has $\gamma \approx 0$. Therefore, the intent is to find x and y (coordinates of the coupler points expressed in E) that lead to the most ill-conditioned matrix $\mathbf{C}$, such that γ is minimized. The Nelder-Mead polytope algorithm may be used for this minimization [49]. Since this algorithm needs as input an initial guess of the parameters to be determined, γ may be plotted in terms of x and y first, in the neighborhood of (0,0)

up to a user-defined range of ϵ. As x and y represent the position of a coupler attachment point with respect to moving refernece frame E, ϵ represents the maximum distance that the coupler attachment points can be from the moving frame E origin. The x and y parameters may then be selected approximately corresponding to the smallest value of γ. These points represent the local minima of the entire γ plot, that is, with $\epsilon = \infty$. However, for practical reasons with ϵ finite, these minima may be regarded as the global minima of the region of interest. At least two minima are required to obtain a planar four-bar mechanism, as each minimum corresponds to a single dyad. The Nelder-Mead algorithm is then fed these approximate values as inputs, and converges to the values of x and y that minimize γ.

Once the values of x and y have been determined, the matrix $\mathbf{C}$ in Equation (4.4) can be populated. The $\mathbf{K}$ parameters may then be estimated using singular value decomposition. The distinction between RR and PR dyads is found by determining whether the resulting $\mathbf{K}$ parameters better describe a circle or line. A resulting circle defines an RR dyad, while a line defines a PR dyad. If Equation (3.11) yields $\mathbf{K}$ parameters defining a circle having dimensions several orders of magnitude greater than the range of the poses, it is recalculated using Equation (3.14) to define a line instead. In this case, the dyad is defined as a PR, rather than an RR.

4.4 RP Dyads

RP dyads pose an interesting special case, as their kinematic constraint is the inverse of PR dyads. Therefore, they must be treated separately. For PR dyads, a fixed point in E is constrained to move on a fixed line in Σ. For an RP dyad, a fixed line in E is constrained to move on a fixed point in Σ. Up till now, Σ has been considered as the fixed coordinate frame, while E has been the moving coordinate frame. However, an RP dyad becomes a

PR dyad by fixing coordinate frame E, such that Σ moves with respect to E. The line in E is now fixed, and the point with fixed coordinates in Σ now moves along it. This is a useful interpretation because we have already worked out a method to find PR dyads. Now we are able to apply that same method to find RP dyads, simply by exchanging the roles of E and Σ.

The implications of this switch in fixed reference frames is that the defined poses must be transformed into the new fixed reference frame. Tranforming the defined poses into the new fixed reference frame entails inverting the original homogeneous transformation matrix given in Equation (3.1). If the coordinates of points in Σ are related to the coordinates of points in E by

$$\begin{bmatrix} X \\ Y \\ Z \end{bmatrix} = \mathbf{T} \begin{bmatrix} x \\ y \\ z \end{bmatrix}, \tag{4.7}$$

then points in E are related to points in Σ by

$$\begin{bmatrix} x \\ y \\ z \end{bmatrix} = \mathbf{T^{-1}} \begin{bmatrix} X \\ Y \\ Z \end{bmatrix}. \tag{4.8}$$

The inverse transformation is then

$$\begin{bmatrix} x \\ y \\ z \end{bmatrix} = \begin{bmatrix} \cos\theta & \sin\theta & -b\sin\theta - a\cos\theta \\ -\sin\theta & \cos\theta & b\cos\theta + a\sin\theta \\ 0 & 0 & 1 \end{bmatrix} \begin{bmatrix} X \\ Y \\ Z \end{bmatrix}. \tag{4.9}$$

Employing this inverse transformation, the RP dyad now behaves as a PR dyad. Furthermore, the revolute joint whose centre has fixed point coordinates in Σ is now constrained to move on a line with fixed line coordinates in E. The roles of Σ and E are completely

reversed. The problem is then finding the constant coordinates of the revolute joint with respect to Σ. The tools for doing so have been previously discussed in Section 4.3. Upon application of this procedure, the RP dyad is determined.

4.5 PP Dyads

Another special case is the PP dyad. Having two prismatic joints in serial restricts the distal rigid body from changing its orientation. This characteristic of PP dyads makes the kinematics involved trivial. Given any set of poses that change in orientation, the PP dyad is immediately ruled out. However, as long as the axes of the two cascaded prismatic joints are not parallel, the PP dyad itself allows the rigid body to undergo any translation. Therefore, given any set of poses with constant orientation, a PP dyad is certain to be one of the dyads that can be paired with another type to achieve the desired motion.

Any PP dyad with nonparallel prismatic axes will allow the desired motion. Therefore, the priority in PP dyad design becomes the practical constraints of the application. The dyad to be paired with may be solved for using the method discussed in this chapter. PP dyads cannot be paired with other PP dyads, unless every two non-sequential prismatic axes are parallel.

In the next section, examples are presented that synthesize dyads of all types, thereby demonstrating the utility and robustness of this new approach to kinematic synthesis of planar four-bar mechanisms.

4.6 Examples

In this chapter, several examples are given that apply the method developed given in Chapter 4. These examples detail the procedure for determining the type and dimensions of dyads which, when paired, will form a planar four-bar mechanism that best approximates

a set of specified poses. In the first example, two RR dyads are synthesized, forming an $RRRR$ mechanism. In the second example, two PR dyads are synthesized, forming the $PRRP$ mechanism intended to be found in 3.6.1. In the third example, two RP dyads are synthesized, forming the $RPPR$ mechanism intended to be found in 3.6.2. In the fourth example, the solution to the McCarthy design challenge [50] is presented, where poses are given without any information with respect to the mechanism that generated them. Finally, in the fifth example, arbitrary poses are used that no planar four-bar mechanism can exactly reproduce. This method will then be applied to an integrated type and dimensional synthesis of the mechanism that best approximates the desired poses in a least squares sense.

4.6.1 RR Dyads

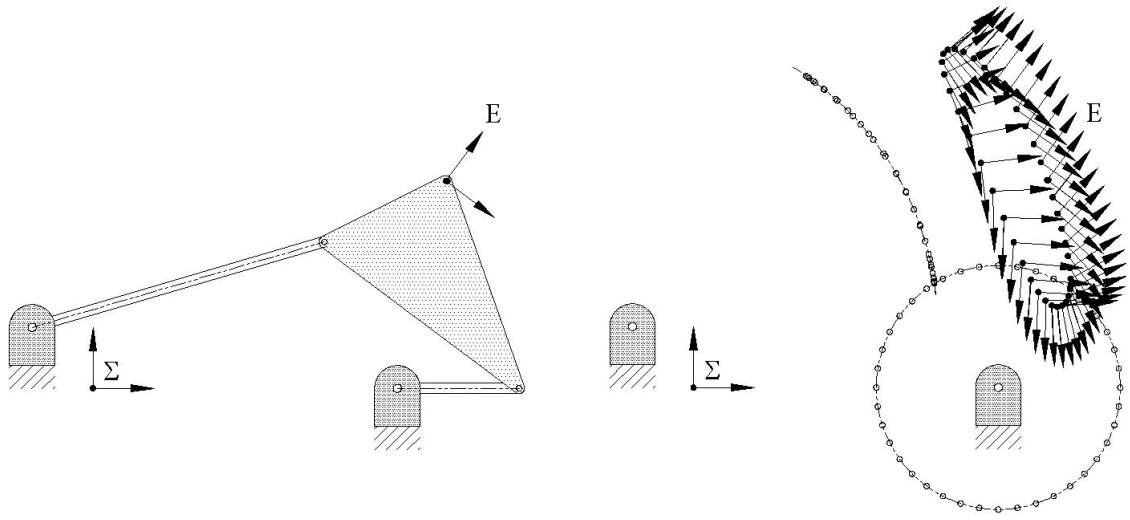

(a) The first pose.

(b) 40 specified poses for E and associated crank and rocker distal R-pair centre locations.

Figure 4.1: The $RRRR$ mechanism.

This first example illustrates how to synthesize RR dyads, and pair them to form an $RRRR$ planar mechanism given more than five poses. 40 poses were used for this example,

and were generated using the $RRRR$ mechanism shown in Figure 4.1(a). The 40 poses are displayed in the figure as well as the configuration of the mechanism in its first pose. In frame E, the rigid body attachment points are (-1, -2) and (3,-2). In this example, as in all others in this chapter, the planar coordinates are given in generic units. The 40 poses are listed in Appendix A.

The first step is to populate $\mathbf{C}$ in Equation (4.3). To begin, we calculate the γ of $\mathbf{C}$ for a range of values of x and y. Many mathematical analysis software packages are capable of computing the condition number κ of a matrix. γ is the inverse of the condition number. The values of x and y are selected such that they minimize γ, thereby ensuring the resulting vectors $\mathbf{K}$ are closest to the nullspace of $\mathbf{C}$. A good tactic is to search an area that contains (0, 0), since for practical mechanisms, the poses should be defined near the rigid body attachment points. For this example, the domains of x and y were taken as $-5 \geq x, y \geq 5$, and data points were computed in increments of 0.05 units to yield the plot of γ shown in Figure 4.2. As can be seen in the figure, there are two distinct minima approximately at points (-1, -2) and (3, -2). These are the two sets of coordinates of (x, y) that make $\mathbf{C}$ the most ill-conditioned. These two sets of points correspond to the two sets of coupler attachment points (x, y) expressed in E. Also, note that the distance between the two minima is the distance between the two coupler attachment points in E. In other words, the distance between the two minima is the coupler length.

Each set of (x, y) is substituted into $\mathbf{C}$, which fully determines the matrix. SVD is then used to factor $\mathbf{C}$ into $\mathbf{U}$, $\mathbf{S}$, and $\mathbf{V}$, as shown in Equation (3.18). The last column of $\mathbf{V}$ is the vector $\mathbf{K}$ that defines the dyad according to Equation (3.11). In this example, the two $\mathbf{K}$ vectors corresponding to the two sets of (x, y) coordinates are listed in Table 4.1. The two $\mathbf{K}$ vectors given in the table define a dyad centered at (-1,1) with link length 5, and a dyad centered at (5,0) with link length 2. This yields the exact generating mechanism shown in Figure 4.1a, and the solution is complete.

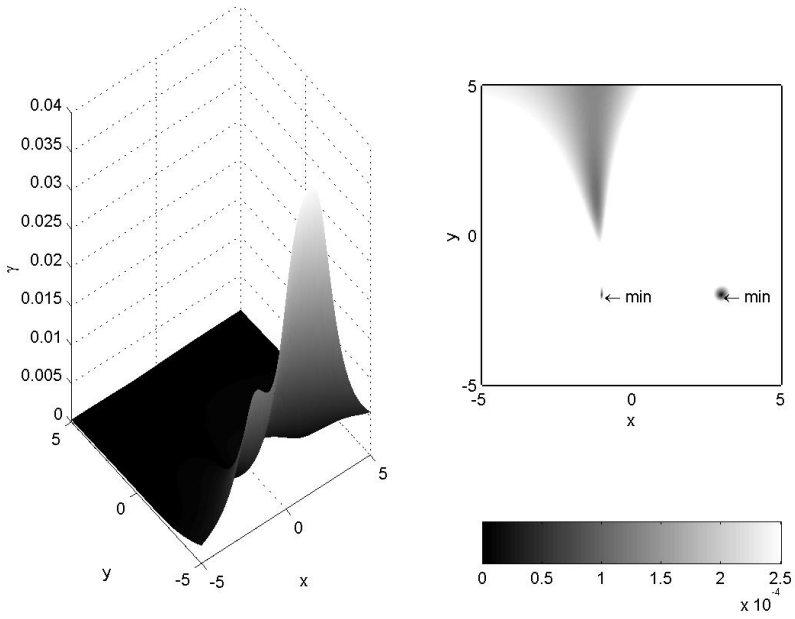

Figure 4.2: γ plot for the poses defined by the *RRRR* mechanism.

	Dyad 1	Dyad 2
x	-1	3
y	-2	-2
K_0	1	1
K_1	1	-5
K_2	-1	0
K_3	23	21

Table 4.1: Parameters defining the *RRRR* mechanism.

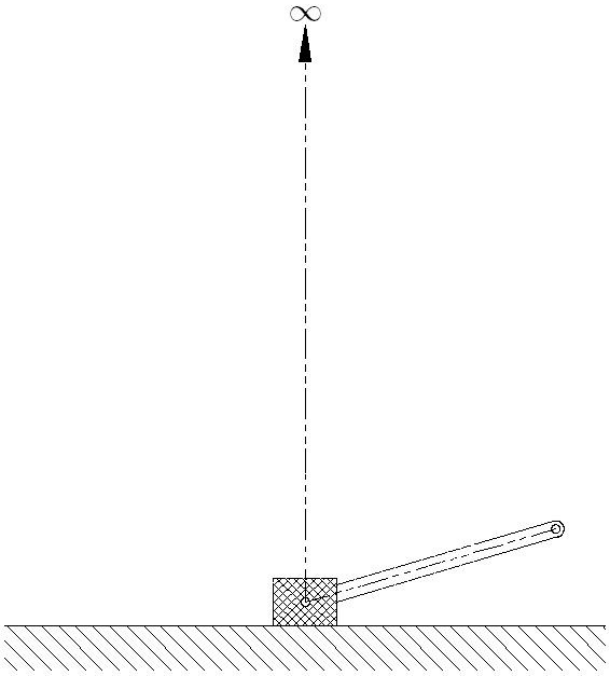

Figure 4.3: A PR dyad.

4.6.2 PR Dyads

Attention is now turned to the PR dyad. PR dyads can be thought of as projectively equivalent to RR dyads with one revolute centre at infinity, and one finite centre. This concept is illustrated in Figure 4.3. Ten poses were used in this example. The mechanism used to generate the ten poses is shown Figure in 4.4. The poses are listed in Table 4.2. The coupler attachment points in E are (-3,-3) and (3,-3). Using the same method as in Section 4.6.1, the values of x and y giving the minimum value of γ are searched for within the square defined by $-5 \leq x, y \leq 5$, in increments of 0.05 units. The resulting plot of γ is shown in Figure 4.5. Figure 4.5 reveals an interesting feature: there are not just two minima, but an entire locus. For now we only consider the minima that we were looking for. It is clear from Figure 4.5 that (-3, -3) and (3, -3) lie on the locus of minima, as indicated by the respective labels min 1 and min 2 in Figure 4.5. Separately substituting those coordinates into **C** and applying SVD results in the **K** vectors given in Table 4.3. It

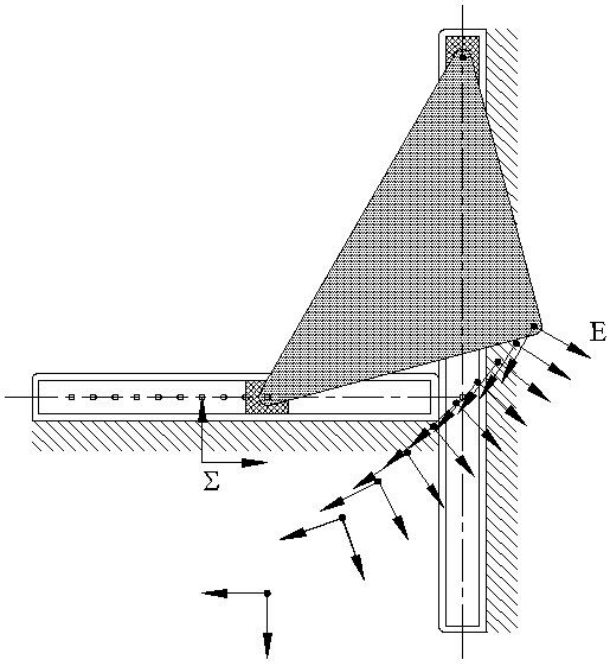

Figure 4.4: The $PRRP$ mechanism.

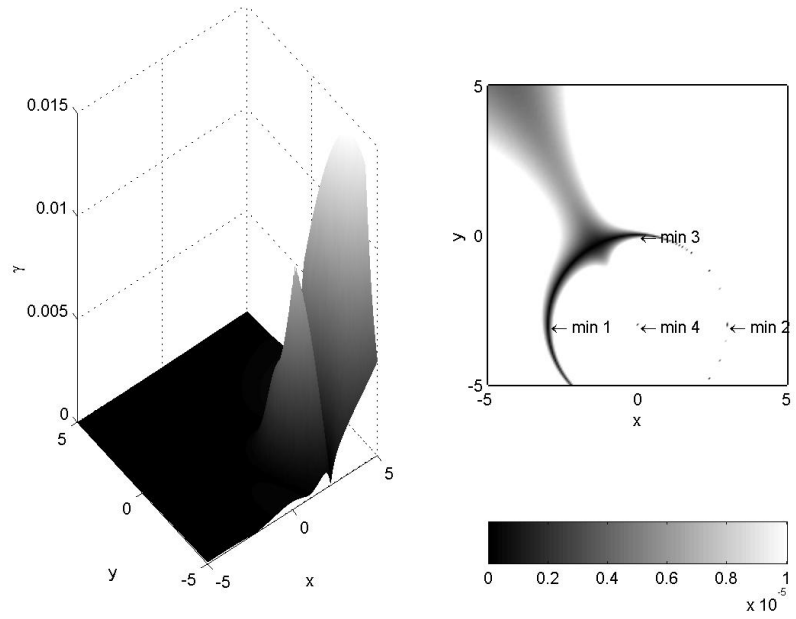

Figure 4.5: γ plot for the $PRRP$ mechanism indicating infinite solutions.

Pose	x	y	θ
1	5.0981	2.0981	-120.0000
2	4.8278	1.8278	-123.7490
3	4.5413	1.5413	-127.6699
4	4.2361	1.2361	-131.8103
5	3.9083	0.9083	-136.2383
6	3.5523	0.5523	-141.0576
7	3.1583	0.1583	-146.4427
8	2.7077	-0.2923	-152.7340
9	2.1527	-0.8473	-160.8119
10	1.0000	-2.0000	-180.0000

Table 4.2: Poses of the $PRRP$ mechanism.

	Dyad 1	Dyad 2
x	-3	3
y	-3	-3
K_0	0	0
K_1	0.1240	0
K_2	0	0.4472
K_3	-0.9923	-0.8944

Table 4.3: Parameters defining the $PRRP$ mechanism.

is clear from the values defining the K_i that the dyads are PR, as both values of K_0 are zero. In order for $\mathbf{K}$ to represent an RR dyad, $\mathbf{K}$ would have to be divided by K_0, yielding infinite values. Using Equation (3.14), the geometry of the two PR dyads are found to be defined by the two lines $X = 4$ and $Y = 1$, with respective attachment points of (-3, -3) and (3, -3) in frame E.

As shown in Figure 4.5, the values of x and y giving the minimum value of γ define a locus of points. This can be explained by the degenerate nature of the mechanism used to generate the points. For example, as discussed earlier, PP dyads confine rigid bodies to a constant orientation. However, any PP dyad may be used to generate rigid body motion of constant orientation. A similar scenario is shown in this example. Because the PR dyad is a special case the RR dyad, the $PRRP$ mechanism constrains the rigid body

	Dyad 1	Dyad 2
x	0	0
y	-3	0
K_0	1	0
K_1	-4	-0.1622
K_2	1	0.1622
K_3	8	-0.9733

Table 4.4: Parameters defining an alternative $RRRP$ mechanism.

in a way that can be produced in many ways.

By using the γ plot given in Figure 4.5, different mechanisms can be synthesized that generate the same motion as that shown in Figure 4.4. For example, using the minima at (0,0) and (0,-3), respectively labelled min 3 and min 4 in Figure 4.5, the two corresponding **K** vectors are found using SVD. The dyads defined by **K** are then found to be those given in Table 4.4. The geometry of the dyads are found to be an RR dyad centred at (4, -1) with link length 3, and a PR dyad defined by the line equation $Y = X - 3$, using Equations (3.11) and (3.14) respectively. The mechanism synthesized by pairing the two dyads is shown in Figure 4.6. The mechanism may not be as practical, as the fixed revolute centre of the RR dyad lies on the fixed prismatic joint of the PR dyad. Nevertheless, the kinematics of the mechanism fit the defined poses, as was meant to be shown. Also, the two dyads can be offset with respect to each other along the z-axis, which will allow the mechanism to move freely without interference.

4.6.3 RP Dyads

Attention is now turned to the RP dyad. RP dyads are kinematic inversions of PR dyads; the difference is that the roles of the moving frame, E, and fixed frame, Σ, of reference are switched. In this example, a mechanism is defined by two fixed lines in E forced to move on two fixed points in Σ, as shown in Figure 4.7. Ten poses generated by the mechanism

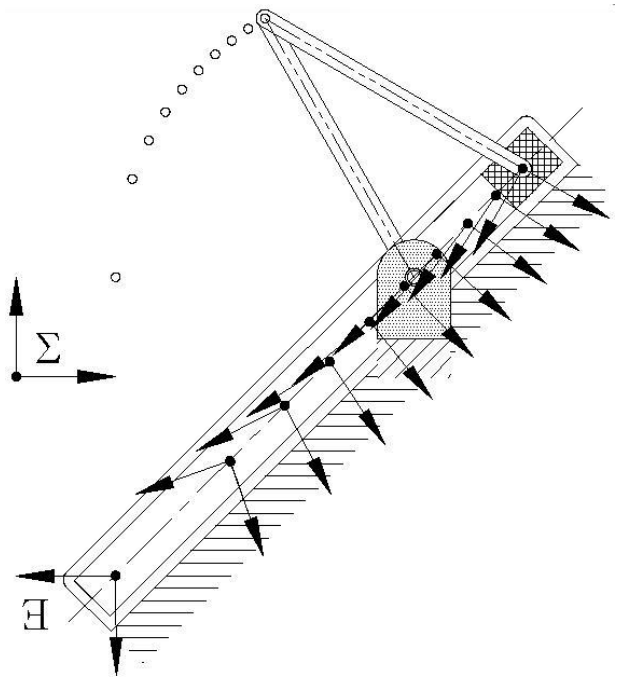

Figure 4.6: An alternative $RRPR$ mechanism.

were used for this example, and are listed in Table 4.5. Plotting γ as a function of x and y reveals no distinct minima. Therefore, no RR or PR dyads can be found that will guide the rigid body through the defined poses. In order to search for RP dyads, the moving frame and fixed frame are switched. Now E is considered as fixed and Σ moves with respect to E. The poses are then transformed using Equation (4.9), so that the poses now describe the motion of Σ with respect to E. Upon transformation of the poses, it is revealed they are identical to the poses defined in the previous example in Section 4.6.2. The solution is then determined to be a $PRRP$ mechanism using the method shown in that section. Once the mechanism is determined, the frames of reference are then exchanged, yielding the generating $RPPR$ mechanism.

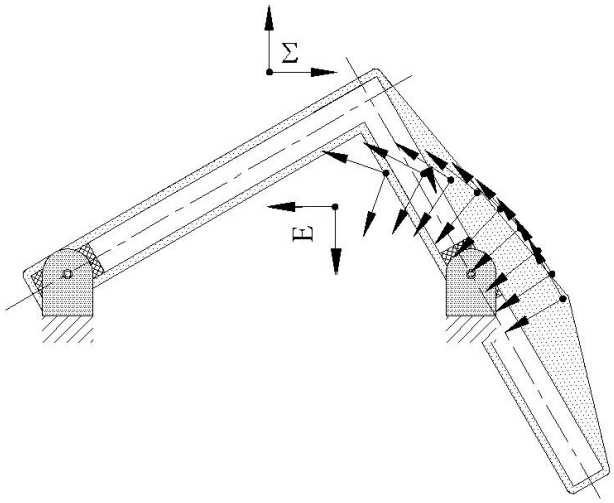

Figure 4.7: The $RPPR$ mechanism.

Pose	x	y	θ
1	4.3660	-3.36602	120.0000
2	4.2018	-2.9988	123.7490
3	3.9952	-2.6527	127.6699
4	3.7454	-2.3333	131.8103
5	3.4509	-2.0472	136.2383
6	3.1100	-1.8032	141.0576
7	2.7194	-1.6139	146.4427
8	2.2729	-1.5003	152.7340
9	1.7546	-1.5078	160.8119
10	1.0000	-2.0000	180.0000

Table 4.5: Poses of the $RPPR$ mechanism.

4.6.4 The McCarthy Design Challenge

This example uses poses taken from J.M. McCarthy's design challenge issued at the ASME DETC Conference in 2002 [50]. In the challenge, no information is given about the mechanism used to generate the poses; in fact, it is possible that no mechanism was used to generate the poses. Without a priori knowledge of the solution, this problem is truly an integrated type and approximate dimensional synthesis problem.

The poses are listed in Table 4.6, and shown graphically in Figure 4.8. Carrying on

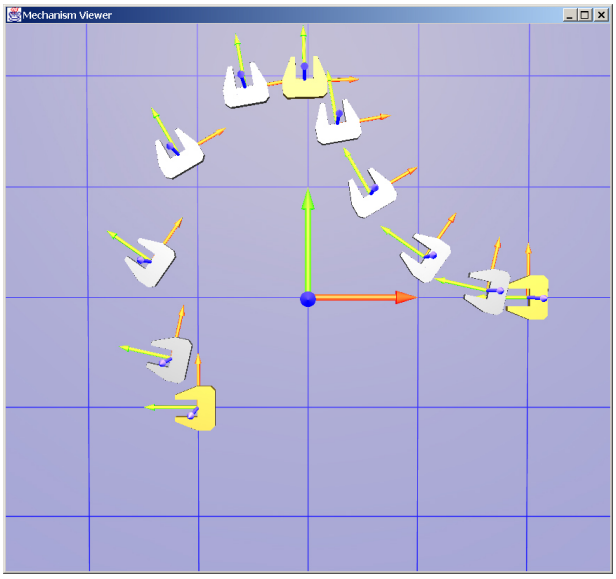

Figure 4.8: McCarthy design challenge poses [50].

in the usual way, the poses are substituted into Equation (4.3) to populate **C**. The γ of **C** are then plotted as functions of x and y, see Figure 4.9. As shown in the figure, two distinct minima occur at approximately (1.5, -0.6) and (1.4, -2.0). Using the Nelder-Mead minimization, the exact values of the two minima are estimated, and listed in Table 4.7. These values are then substituted into Equation (4.3) to completely determine **C**. SVD is then applied to **C** to find **K** corresponding to each minimum. The values of **K** determined for this problem are also given in Table 4.7. With the two dyads synthesized, the problem is now solved. The mechanism is composed of two RR dyads centred on (0.7860, 0.3826) and (2.2153, 1.6159), with respective link lengths of 1.7330 and 1.7307. The synthesized $RRRR$ mechanism solving the problem is illustrated in Figure 4.10.

4.6.5 General problem

Attention is now turned to an example that requires completely general integrated type and approximate dimensional synthesis. By defining poses that are impossible to generate exactly by any four-bar planar mechanism, this method is put to the test. The poses used

Pose	x	y	θ
1	-1.0000	-1.0000	90.0000
2	-1.2390	-0.5529	77.3621
3	-1.4204	0.3232	55.0347
4	-1.1668	1.2858	30.1974
5	-0.5657	1.8871	10.0210
6	-0.02927	1.9547	1.7120
7	0.2632	1.5598	10.0300
8	0.5679	0.9339	30.1974
9	1.0621	0.3645	55.0346
10	1.6311	0.0632	77.3620
11	2.0000	0.0000	90.0000

Table 4.6: Poses given in the McCarthy design challenge.

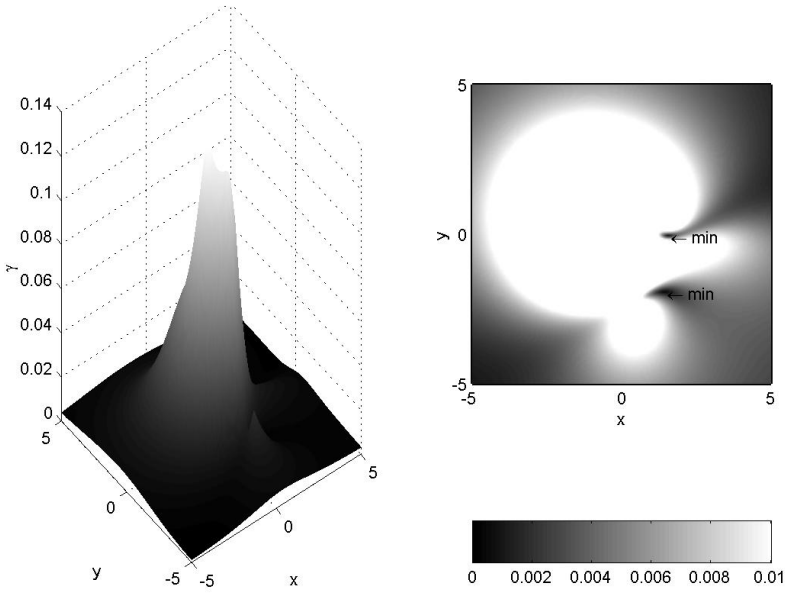

Figure 4.9: γ plot for the design poses.

	Dyad 1	Dyad 2
x	1.5656	1.4371
y	-0.0583	-1.9415
K_0	1	1
K_1	-0.7860	-2.2153
K_2	-0.3826	-1.6159
K_3	-2.2390	4.5236

Table 4.7: Parameters defining a solution to the defined poses.

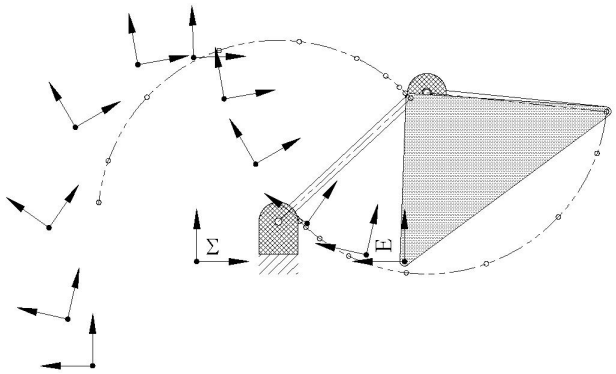

Figure 4.10: *RRRR* solving the McCarthy design challenge.

in this example define a square corner. A point on the rigid body moves linearly between the Cartesian coordinates from (0, 1) to (1, 0) via (1,1). The orientation increases linearly from 0 to 90 degrees. The poses are given in Table 4.8, and shown graphically in Figure 4.11. A planar four-bar mechanism cannot exactly replicate the motion defined above, because points on the coupler generate either a 6^{th}, 4^{th}, or 2^{nd} order curve. The curve

$$x^n + y^n = 1 \tag{4.10}$$

is plotted for various values of n in Figure 4.12, where n defines the order of the curve. As shown in the figure, the higher order the curve, the better the curve approximates a square corner. However, an exactly square corner requires $n = \infty$. With $n \leq 6$ for planar four-bar mechanisms, it is impossible to exactly replicate the desired motion. Although a

Pose	x	y	θ
1	0.0	1.0	0.0
2	0.1	1.0	4.5
3	0.2	1.0	9.0
4	0.3	1.0	13.5
5	0.4	1.0	18.0
6	0.5	1.0	22.5
7	0.6	1.0	27.0
8	0.7	1.0	31.5
9	0.8	1.0	36.0
10	0.9	1.0	40.5
11	1.0	1.0	45.0
12	1.0	0.9	49.5
13	1.0	0.8	54.0
14	1.0	0.7	58.5
15	1.0	0.6	63.0
16	1.0	0.5	67.5
17	1.0	0.4	72.0
18	1.0	0.3	76.5
19	1.0	0.2	81.0
20	1.0	0.1	85.5
21	1.0	0.0	90.0

Table 4.8: Numerical representation of the poses defining a square corner.

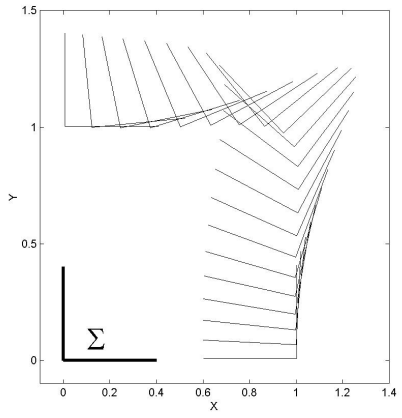

Figure 4.11: Graphical representation of the poses defined for this example.

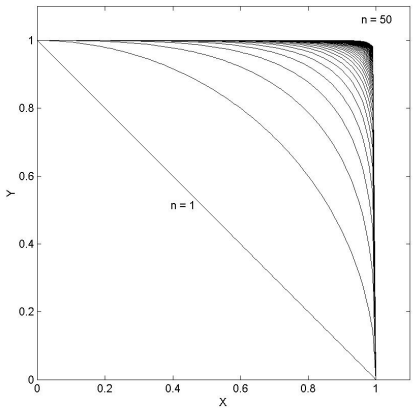

Figure 4.12: n^{th} order curves.

$PPPP$ mechanism may be able to generate the desired point translation, the linear change in orientation rules out this type of mechanism since it is unable to change its orientation. As in the previous examples, the pose data are substituted into Equation (4.3) to populate $\mathbf{C}$. The γ of $\mathbf{C}$ is then plotted as a function of x and y and is illustrated in Figure 4.13. As can be seen in Figure 4.13, two distinct minima occur at approximately (0.8, 0.6) and (0.8, -0.6). Using the Nelder-Mead minimization and the pair of approximate x and y as initial guesses, the exact values of the two minima are found, and listed in Table 4.9. These values are then substituted into Equation (4.3) to completely determine $\mathbf{C}$. Then SVD

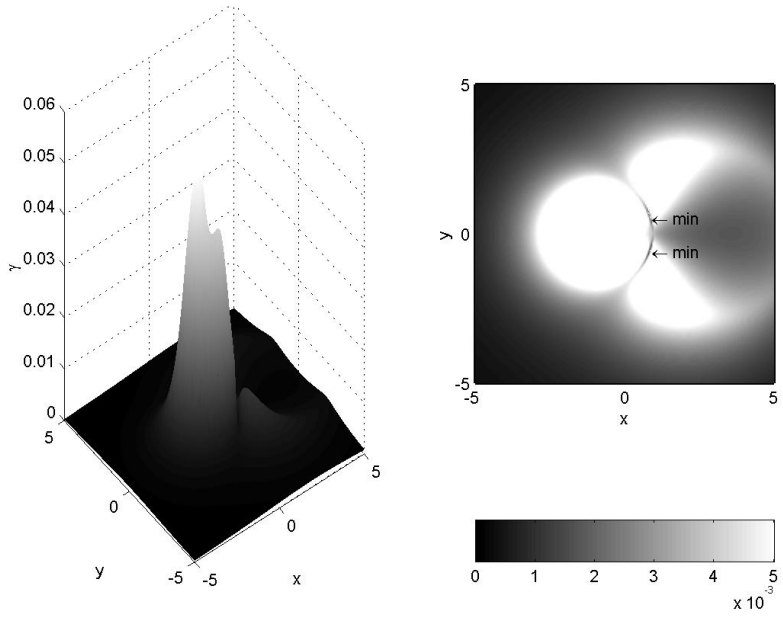

Figure 4.13: γ plot the poses defining a square corner.

can be applied to **C** to find **K** corresponding to each minimum. The values of **K** thus determined are in Table 4.9. With the parameters defining the two dyads determined, the problem is now solved. The mechanism is composed of two RR dyads centred on (4.5843, -1.0539) and (-1.0539, 4.5843), both with links having length 1.7307. The $RRRR$ mechanism solving the problem is shown in Figure 4.14. As this example was truly an approximate synthesis problem, it is interesting to see how well the synthesized mechanism approximates the desired poses. Figure 4.15 shows the positional and orientation output

	Dyad 1	Dyad 2
x	0.8413	0.8413
y	0.5706	-0.5706
K_0	1	1
K_1	-4.5843	1.0539
K_2	1.0539	-4.5843
K_3	1.2704	1.2704

Table 4.9: Parameters defining the solution to the general problem.

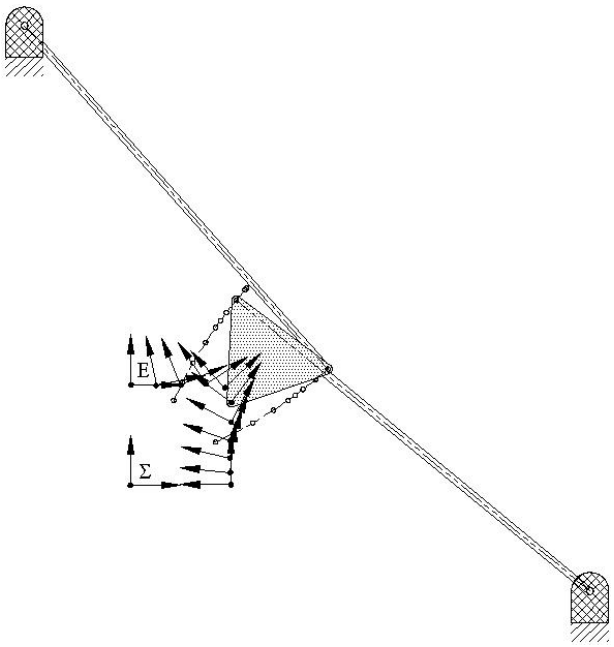

Figure 4.14: *RRRR* mechanism approximating the poses in Table 4.8.

	Position	Orientation
Average Error	0.1092	5.0225°
Residual Norm	0.5615	26.1086°

Table 4.10: Error statistics of the *RRRR* mechanism.

of the mechanism compared to the intended output. This is known as the *structural error*. The statistics of the error are listed in Table 4.10, where the residual norm is defined as

$$norm = \|\mathbf{x}\| = \sqrt{\sum \left(x_{desired} - x_{actual}\right)^2}. \tag{4.11}$$

As shown in the figures, the output for both position and orientation closely match the defined poses. A plot of the output error with respect to the design poses is given in Figure 4.16. As these poses were defined arbitrarily, without any a priori knowledge regarding type or dimensions for feasible mechanisms, this method has proven its capabilities for integrated type and approximate dimensional synthesis.

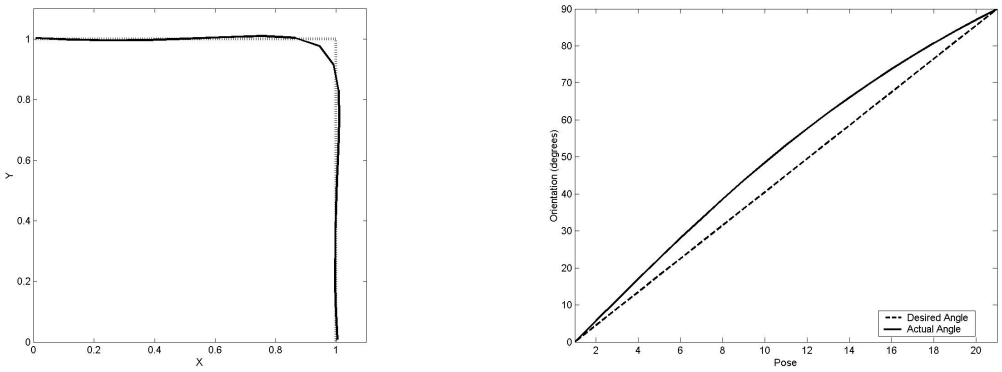

(a) Positional. (b) Orientation.

Figure 4.15: Output of the *RRRR* mechanism.

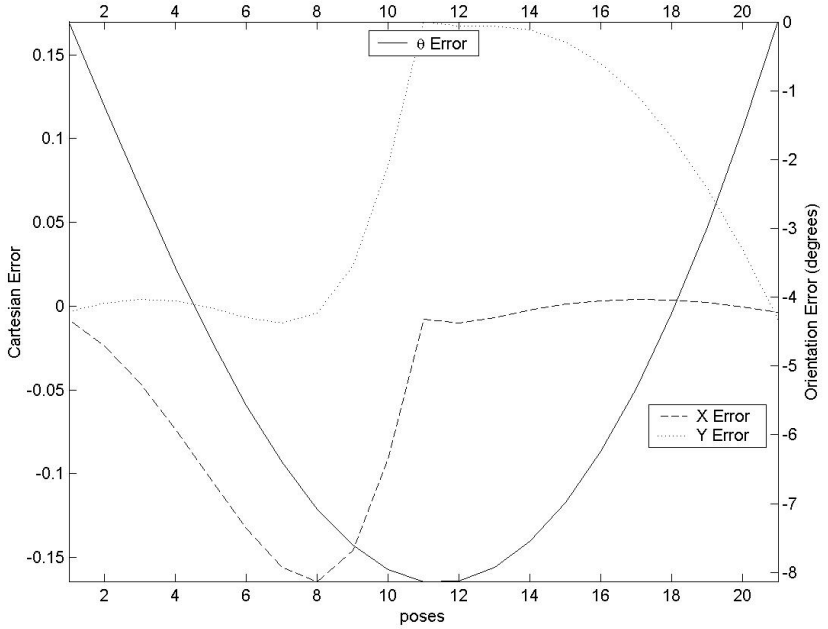

Figure 4.16: *RRRR* mechanism pose error.

Chapter 5

Conclusions and Recommendations

This thesis presents two methods that integrate type and approximate dimensional synthesis of planar four-bar mechanisms for rigid-body guidance. Attempts were made to first linearize the problem in order to apply linear numerical techniques, using kinematic mapping. Unfortunately, this approach led to the exclusion of general RR dyads being determined, except for some special cases. Furthermore, application of this technique has yielded limited success for approximate synthesis in general. I.e., in the examples given, the determined dyad does not match either of the dyads used to generate the poses. Clearly, this method offers potential for success, but much more work is required.

The second method was then presented which successfully solves the integrated type and approximate dimensional synthesis problem for planar four-bar mechanisms used for rigid-body guidance. By using a novel approach in which coupler attachment points are correlated between moving frame E and fixed frame Σ, the number of independent variables defining a suitable dyad for the desired poses is reduced from five to two. Numerical methods are then used to solve for both type and approximate dimensions of this much simplified problem. Several examples were presented as proof-of-concept towards its utility and robustness.

There are several recommendations for further work on these two methods. For the kinematic mapping method, further investigation is warranted regarding why two dyads were unable to be determined, even with a synthesis matrix rank deficiency of two. Furthermore, investation into why the determined dyad does not match either of the dyads used to generate the poses in the examples would also prove insightful. In all examples using this method, the determined dyad always has its coupler attachment point at $(0, 0)$ in the moving reference frame E. Perhaps this is a limitation of the method, or the gateway to its successful modification.

Regarding the successful synthesis technique, a sensitivity analysis would prove to be insightful. In the analysis, pose sensitivity to deviations in mechanism dimensions could be determined with respect to the coupler attachment points (x, y) in moving frame E. It is hypothesized that pose sensitivity increases with the magnitude of (x, y). The reasoning is that dimensional deviations give rise to errors multiplied by the distance of moving frame E to the coupler attachment point, which acts as a moment arm. It is for this reason that the search for γ minima is restricted to the neighborhood of $(0, 0)$. No other choices would yield practical results. However, a formal study investigating the principle of this hypothesis would settle the matter. In general, it would also provide insight into mechanism sensitivity to error, which would prove useful in the practical application of mechanism sythesis, especially in regards to mechanism manufacturing.

References

[1] M.J.D. Hayes, T. Luu, and X.-W. Chang. "Kinematic Mapping Application to Approximate Type and Dimension Synthesis of Planar Mechanisms". *9th Advances in Robotic Kinematics,* eds. Lenarčič, J. and Galletti, C., Kluwer Academic Publishers, Dordrecht, the Netherlands, pages 41–48, June 28 - July 1, 2004.

[2] T. Luu and M.J.D. Hayes. "Integrated Type and Approximate Dimensional Synthesis of Planar Four-Bar Mechanisms for Rigid Body Guidance". *The Canadian Committee for the Theory of Machines and Mechanisms Symposium on Mechanisms, Machines, and Mechatronics,* Saint-Hubert, Quebec, May 26 - 27, 2005.

[3] L. Burmester. *Lehrbuch der Kinematik.* Arthur Felix Verlag, Leipzig, Germany, 1888.

[4] J. Vallejo, R. Aviles, A. Hernandez, and E. Amezua. "Nonlinear Optimization of Planar Linkages for Kinematic Syntheses". *Mechanism and Machine Theory*, 30(4):501–518, 1995.

[5] R. Aviles, M. Ajuria, J. Vallejo, and A. Hernandez. "A Procedure for the Optimal Synthesis of Planar Mechanisms Based on Non-Linear Position Problems". *International Journal for Numerical Methods In Engineering*, 40(8):1505–1524, 1997.

[6] R. Aviles, S. Navalpotro, E. Amezua, and A. Hernandez. "An Energy-Based General-Method for the Optimum Synthesis of Mechanisms". *Journal of Mechanical Design*, 116(1):127–136, 1994.

[7] R. Akhras and J. Angeles. "Unconstrained Nonlinear Least-Square Optimization of Planar Linkages for Rigid-Body Guidance". *Mechanism and Machine Theory*, 25(1):97–118, 1990.

[8] P.S. Shiakolas, D. Koladiya, and J. Kebrle. "On the Optimum Synthesis of Four-Bar Linkages Using Differential Evolution and the Geometric Centroid of Precision Positions". *Inverse Problems In Engineering*, 10(6):485–502, 2002.

[9] S. Krishnamurty and D. Turcic. "Optimal Synthesis of Mechanisms Using Nonlinear Goal Programming Techniques". *Mechanism and Machine Theory*, 27(5):599–612, 1992.

[10] P. Larochelle and J.M. McCarthy. "Designing Planar Mechanisms Using a Bi-Invariant Metric in the Image Space of SO". *American Society of Mechanical Engineers, Design Engineering Division, 23rd Biennial Mechanisms Conference*, 70(1):221–228, 1994.

[11] P. Larochelle and J.M. McCarthy. "Planar Motion Synthesis Using an Approximate Bi-Invariant Metric". *Journal of Mechanical Design*, 117(4):646–651, 1995.

[12] S. Krishnamurty J. Mariappan. "A Generalized Exact Gradient Method for Mechanism Synthesis". *Mechanism and Machine Theory*, 31(4):413–421, 1996.

[13] R. Sancibrian, P. Garcia, F. Viadero, and A. Fernandez. "Exact-Gradient Optimization Method for Rigid-Body Guidance Synthesis in Planar Mechanisms". *Proceedings of the ASME Design Engineering Technical Conference and Computers and Information in Engineering Conference 2004: Volume 2: 28th Biennial Mechanisms and Robotics Conference*, pages 155–161, 2004.

[14] X. Zhang, J. Zhou, and Y. Ye. "Optimal Mechanism Design Using Interior-Point Methods". *Mechanism and Machine Theory*, 35(1):83–98, 2000.

[15] P.M. Larochelle. "Approximate Motion Synthesis of Open and Closed Chains Via Parametric Constraint Manifold Fitting: Preliminary Results". *Proceedings of the ASME Design Engineering Technical Conferences and Computers and Information in Engineering Conference*, 2:1049–1057, 2003.

[16] J. Alba, M. Doblare, and L. Gracia. "A Simple Method for the Synthesis of 2D and 3D Mechanisms with Kinematic Constraints". *Mechanism and Machine Theory*, 35(5):645–674, 2000.

[17] Z. Wang, H. Yu, D. Tang, and J. Li. "Study on Rigid-Body Guidance Synthesis of Planar Linkage". *Mechanism and Machine Theory*, 37(7):673–684, 2002.

[18] J. Yao and J. Angeles. "Computation of All Optimum Dyads in the Approximate Synthesis of Planar Linkages for Rigid-Body Guidance". *Mechanism and Machine Theory*, 35(8):1065–1078, 2000.

[19] A. Liu and T. Yang. "Finding All Solutions to Unconstrained Nonlinear Optimization for Approximate Synthesis of Planar Linkages Using Continuation Method". *Journal of Mechanical Design*, 121(3):368–374, 1999.

[20] X. Kong. "Approximate Kinematic Synthesis of Linkages Using Generalized Inverse Matrix and Continuation". *Mechanical Science and Technology*, 18(1):38–40, 1999.

[21] J.P. Modak and P.M. Padole. "Establishing the Minimum and Necessary Condition for Synthesis of an Adjustable Planer Four-Bar Mechanism for the Six Positions Rigid Body Guidance". *Modelling, Simulation & Control B: Mechanical & Thermal Engineering, Materials & Resources, Chemistry*, 19(3):53–64, 1988.

[22] S.N. Kramer. *"Selective Precision Synthesis of Planar Mechanisms Satisfying Practical Design Requirements"*. PhD thesis, Rensselaer Polytechnic Institute, 'Troy, New York, 1973.

[23] K.Y. Kim. "Modified Selective Precision Synthesis Technique for Planar Four-Bar Rigid-Body Guidance". *Proceedings of the Institution of Mechanical Engineers, Part C: Journal of Mechanical Engineering Science*, 209(1):39–47, 1995.

[24] A. Vasiliu and B. Yannou. "Dimensional Synthesis of Planar Mechanisms Using Neural Networks: Application to Path Generator Linkages". *Mechanism and Machine Theory*, 36(2):299–310, 2001.

[25] J.C. Hoskins and G.A. Kramer. "Synthesis of Mechanical Linkages Using Artificial Neural Networks and Optimization". *IEEE International Conference on Neural Networks*, 2:822, 1993.

[26] G. Roston and R. Sturges. "Genetic Algorithm Synthesis of Four-Bar Mechanisms". *AI Edam-Artificial Intelligence for Engineering Design Analysis and Manufacturing*, 10(5):371–390, 1996.

[27] J. Cabrera, A. Simon, and M. Prado. "Optimal Synthesis of Mechanisms with Genetic Algorithms". *Mechanism and Machine Theory*, 37(10):1165–1177, 2002.

[28] A. Bose, M. Gini, and D. Riley. "A Case-Based Approach to Planar Linkage Design". *Artificial Intelligence In Engineering*, 11(2):107–119, 1997.

[29] X. Wu. "Study on Dimension Synthesis of Planar Linkages for Rigid-Body Guidance with Prescribed Timing". *Chinese Journal of Mechanical Engineering*, 35(5):106–110, 1999.

[30] X. Wu. "Optimal Dimension Synthesis of Planar Linkages for Rigid-Body Guidance with Prescribed Timing". *Chinese Journal of Mechanical Engineers*, 37(12):34–36, 2001.

[31] W. Blashke. "Euklidische Kinematik und Nichteuklidische Geometrie". *Zeitschr. Math. Phys.*, 60:61–91 and 203–204, 1911.

[32] J. Grunwald. "Ein Abbildungsprinzip, Welches die ebene Geometrie und Kinematik mit der Raumlichen Geometrie Verknupft". *Sitzber. Ak. Wiss. Wien*, 120:667–741, 1911.

[33] B. Ravani and B. Roth. "Motion Synthesis Using Kinematic Mappings". *Journal of Mechanisms, Transmissions, and Automation in Design*, 105(3):460–467, 1983.

[34] B. Ravani. *Kinematic Mappings as Applied to Motion Approximation and Mechanism Synthesis*. PhD thesis, Stanford University, Stanford, CA, 1982.

[35] M.J.D. Hayes and P.J. Zsombor-Murray. "Solving the Burmester Problem Using Kinematic Mapping". *Proc. of the ASME Design Engineering Technical Conferences: Mechanisms Conference,* Montreal, QC, 2002.

[36] M.J.D. Hayes and P.J. Zsombor-Murray. "Towards Integrated Type and Dimensional Synthesis of Mechanisms for Rigid Body Guidance". *Proceedings of the CSME Forum 2004*, pages 53–61, June 1-4, 2004.

[37] K.H. Hunt. *Kinematic Geometry of Mechanisms*. Clarendon Press, Oxford, England, 1978.

[38] S. Roberts. "On the Motion of A Plane Under Certain Conditions". *Proceedings of the London Mathematics Society*, 3:286–318, 1871.

[39] R. Beyer. *Kinematische Getriebesynthese*. Springer, Berlin, 1953.

[40] R.S. Hartenberg and J. Denavit. *Kinematic Synthesis of Linkages*. McGraw-Hill, Book Co., New York, N.Y., U.S.A., 1964.

[41] O. Bottema and B. Roth. *Theoretical Kinematics*. Dover Publications, Inc., New York, N.Y., 1990.

[42] M.J.D. Hayes and M.L. Husty. "On the Kinematic Constraint Surfaces of General Three-Legged Planar Robot Platforms". *Mechanism and Machine Theory*, 38(5):379–394, 2003.

[43] M.J.D. Hayes, P.J. Zsombor-Murray, and C. Chen. "Unified Kinematic Analysis of General Planar Parallel Manipulators". *ASME Journal of Mechanical Design*, 126(5):866–874, 2004.

[44] F. Klein. *Elementary Mathematics from an Advanced Standpoint: Geometry*. Dover Publications, Inc., New York, N.Y., 1939.

[45] G.H. Golub and C.F. Van Loan. *Matrix Computations, third edition*. the John Hopkins University Press, Baltimore, MD, 1996.

[46] W.H. Press, S.A. Teukolsky, W.T. Vetterling, and B.P. Flannery. *Numerical Recipes in C, 2nd Edition*. Cambridge University Press, Cambridge, England, 1992.

[47] E. Anderson, Z. Bai, C. Bischof, S. Blackform, J. Demmel, J. Dongarra, J. Du Croz, A. Greenbaum, S. Hammarling, A. McKenney, and D. Sorensen. *LAPACK User's Guide, third edition*. Society for Industrial and Applied Mathematics, Philadelphia, PA, 1999.

[48] G. Strang. *Linear Algebra and its Applications*. Academic Press, 1980.

[49] J. A. Nelder and R. Mead. "A Simplex Method for Function Minimization". *Computer Journal*, 7:308–313, 1965.

[50] J.M. McCarthy. The McCarthy Design Challenge. ASME Design Engineering Technical Conference, 2002.

Appendix A

The 40 Poses for Example in Section 4.6.1

Pose	x	y	θ	Pose	x	y	θ
1	5.8000	3.4000	-36.8699	21	5.0885	2.7827	-91.5809
2	5.6975	3.6928	-35.5743	22	5.2523	2.3824	-93.7945
3	5.5804	3.9899	-34.8906	23	5.3998	2.0416	-94.7136
4	5.4469	4.2831	-34.7651	24	5.5342	1.7685	-94.4070
5	5.2968	4.5637	-35.1406	25	5.6581	1.5643	-93.0169
6	5.1321	4.8231	-35.9676	26	5.7724	1.4256	-90.7145
7	4.9564	5.0530	-37.2105	27	5.8764	1.3468	-87.6706
8	4.7756	5.2463	-38.8495	28	5.9686	1.3214	-84.0422
9	4.5972	5.3966	-40.8801	29	6.0468	1.3429	-79.9682
10	4.4301	5.4986	-43.3116	30	6.1089	1.4053	-75.5712
11	4.2844	5.5476	-46.1645	31	6.1531	1.5029	-70.9616
12	4.1703	5.5394	-49.4669	32	6.1783	1.6305	-66.2420
13	4.0982	5.4704	-53.2478	33	6.1843	1.7838	-61.5124
14	4.0765	5.3368	-57.5262	34	6.1716	1.9594	-56.8740
15	4.1109	5.1351	-62.2929	35	6.1417	2.1549	-52.4330
16	4.2018	4.8634	-67.4853	36	6.0965	2.3689	-48.3003
17	4.3425	4.5234	-72.9570	37	6.0384	2.6009	-44.5878
18	4.5193	4.1234	-78.4578	38	5.9693	2.8508	-41.3983
19	4.7136	3.6816	-83.6426	39	5.8900	3.1179	-38.8115
20	4.9074	3.2247	-88.1280	40	5.8000	3.4000	-36.8699

Table A.1: Poses of the *RRRR* mechanism.

Appendix B

Source Code for Kinematic Mapping Method

```
function []=linearize(poses)
   c=pi/180;
   x1=poses(:,1);
   y1=poses(:,2);
   theta=poses(:,3);
   X4=2*cos(theta*c/2);
   X1=(x1.*sin(theta*c/2)-y1.*cos(theta*c/2))./X4;
   X2=(x1.*cos(theta*c/2)+y1.*sin(theta*c/2))./X4;
   X3=2*sin(theta*c/2)./X4;
   X4=2*cos(theta*c/2)./X4;
   C=[X2+X1.*X3 X2.*X3-X1 1/4*(1+X3.^2) 1/2*(1-X3.^2) X3];
   [U,S,V]=svd(C);
   kappa=V(:,5)
   K1=kappa(1);
```

```
K2=kappa(2);

K3=kappa(3);

C2=[K1 K2;K2 -K1];

a=C2[kappa(4);kappa(5)];

x=a(1)

y=a(2)
```

Appendix C

Source Code for Complete and General Method

```
function [gamma] = mymethod(poses)
   global theta x1 y1 sizex
   c=pi/180;
   sizex = size(x,1);
   x1=poses(:,1);
   y1=poses(:,2);
   theta=poses(:,3);
   i=1;
   for xe=-5:.05:5
   for ye=-5:.05:5
   gamma(i)=1/cond([(cos(theta*c)*xe-sin(theta*c)*ye+x1).^2+...
   (sin(theta*c)*xe+cos(theta*c)*ye+y1).^2
   2*(cos(theta*c)*xe-sin(theta*c)*ye+x1)
   2*(sin(theta*c)*xe+cos(theta*c)*ye+y1)
```

```
ones(sizex,1)]);
i=i+1;
end
xe
end
size(gamma)
gamma=reshape(gamma,201,[]);
[x,out] = fminsearch('xeyefcn',[-3, -3]);
xe=x(1);
ye=x(2);
gamma2=1/cond([(cos(theta*c)*xe-sin(theta*c)*ye+x1).^2+...
(sin(theta*c)*xe+cos(theta*c)*ye+y1).^2
2*(cos(theta*c)*xe-sin(theta*c)*ye+x1)
2*(sin(theta*c)*xe+cos(theta*c)*ye+y1)
ones(sizex,1)]);
[U,S,V]=svd([(cos(theta*c)*xe-sin(theta*c)*ye+x1).^2+...
(sin(theta*c)*xe+cos(theta*c)*ye+y1).^2
2*(cos(theta*c)*xe-sin(theta*c)*ye+x1)
2*(sin(theta*c)*xe+cos(theta*c)*ye+y1)
ones(sizex,1)]);
K=V(:,4)/V(1,4)
[x,out] = fminsearch('xeyefcn',[3, -3]);
xe=x(1);
ye=x(2);
gamma2=1/cond([(cos(theta*c)*xe-sin(theta*c)*ye+x1).^2+...
(sin(theta*c)*xe+cos(theta*c)*ye+y1).^2
```

```
2*(cos(theta*c)*xe-sin(theta*c)*ye+x1)

2*(sin(theta*c)*xe+cos(theta*c)*ye+y1)

ones(sizex,1)]);

[U,S,V]=svd([(cos(theta*c)*xe-sin(theta*c)*ye+x1).^2+...

(sin(theta*c)*xe+cos(theta*c)*ye+y1).^2

2*(cos(theta*c)*xe-sin(theta*c)*ye+x1)

2*(sin(theta*c)*xe+cos(theta*c)*ye+y1)

ones(sizex,1)]);

K=V(:,4)/V(1,4)
```